

# A global Budyko model to partition evaporation into interception and transpiration

Ameneh Mianabadi<sup>1,2</sup>, Miriam Coenders–Gerrits<sup>2\*</sup>, Pooya Shirazi<sup>1</sup>, Bijan Ghahraman<sup>1</sup>,  
Amin Alizadeh<sup>1</sup>

1- Water Engineering Department, Faculty of Agriculture, Ferdowsi University of  
Mashhad, Mashhad, Iran

2- Water Resources Section, Faculty of Civil Engineering and Geosciences, Delft  
University of Technology, Delft, The Netherlands

\*Corresponding author

## Abstract

Evaporation is a crucial flux in the hydrological cycle and links the water and energy balance of a catchment. The Budyko framework is often used to provide a first order estimate of evaporation, as it is a straightforward model with only rainfall and potential evaporation as required input. Many researchers have improved the Budyko framework by including more physics and catchment characteristics into the original equation. However, the parameterization of these improved Budyko models is not so straightforward, data demanding, and requires local knowledge that is difficult to obtain at the global scale. In this paper we present an improvement of the previously presented Gerrits' model ("Analytical derivation of the Budyko curve based on rainfall characteristics and a simple evaporation model" in Gerrits et al, 2009 WRR), whereby total evaporation is calculated on the basis of simple interception and transpiration thresholds in combination with measurable parameters like rainfall dynamics and storage availability from remotely sensed data sources. While Gerrits' model was previously investigated for 10 catchments with different climate conditions and where some parameters were assumed to be constant, in this study we applied the model at the global scale and fed the model with remotely sensed input data. The output of the model has been compared to two complex land-surface models, STEAM and GLEAM, as well as the database of Landflux-EVAL. Our results show that total evaporation estimated by Gerrits' model is in good agreement with Landflux-EVAL, STEAM and GLEAM. The results also show that Gerrits' model underestimates interception in comparison to STEAM and overestimates it in comparison to GLEAM, whereas the opposite is found for transpiration. Errors in interception can partly be explained by differences in the definition of interception that successively introduce errors in the calculation of transpiration. Relating to the Budyko framework, the model shows a reasonable performance for the estimation of total evaporation. The results also found a unimodal distribution of the transpiration to precipitation fraction ( $\frac{E_t}{P}$ ), indicating that both increasing and decreasing aridity will result in a decline in the fraction of transpired rainfall by plants for growth and metabolism.

**Keywords:** Budyko curves, interception, transpiration, remote sensing, evaporation

## 1. Introduction

1 Budyko curves are used as a first order estimate of annual evaporation in terms of annual  
2 precipitation and potential evaporation. If the available energy is sufficient to evaporate the  
3 available moisture, annual evaporation can approach annual precipitation (water-limited  
4 situation). If the available energy is not sufficient, annual evaporation can approach potential  
5 evaporation (energy-limited situation). Using the water balance and the energy balance and by  
6 applying the definition of the aridity index and Bowen ratio, the Budyko framework can be  
7 described as (Arora, 2002):

$$\frac{E_a}{P_a} = \frac{\phi}{1+f(\phi)} = F(\phi) \quad (1)$$

8 with  $E_a$  annual evaporation [L/T],  $P_a$  annual precipitation [L/T],  $\frac{E_a}{P_a}$  the evaporation ratio [-], and  
9  $\phi$  the aridity index, which is defined as the potential evaporation divided by annual precipitation  
10 [-]. All Budyko curves, developed by different researchers (Table 1), have a similar pattern as  
11 Eq. (1).

12 The equations shown in Table 1 assume that the evaporation ratio is determined by climate only  
13 and do not take into account the effect of other controls on the water balance. Therefore, some  
14 researchers incorporated more physics into the Budyko framework. For example, Milly (1994,  
15 1993) investigated the root zone storage as an essential secondary control on the water balance.  
16 Choudhury (1999) used net radiation and a calibration factor in the Budyko curves. Zhang et al.  
17 (2004, 2001) tried to add a plant-available water coefficient, Porporato et al. (2004) took into  
18 account the maximum storage capacity, Yang et al. (2006, 2008) incorporated a catchment  
19 parameter, and Donohue et al. (2007) tried to consider vegetation dynamics. The inclusion of  
20 these physics and catchments characteristics improved the performance of the Budyko curves  
21 locally; however, it made them less applicable for the global scale, since the parameterisation is  
22 data demanding and requires local knowledge, which is not always available. Therefore, in this  
23 study, we aim to show that the Budyko framework can also be explained with a simple analytical  
24 model that is less depending on local data that is difficult to obtain at the global scale.  
25 Accordingly, we use the reasoning of the model of Gerrits et al. (2009) (hereafter Gerrits'  
26 model) that recognizes the characteristic time scales of the different evaporation processes (i.e.  
27 interception at daily scale and transpiration at monthly scale). Despite the fact that Gerrits et al.  
28 (2009) aimed to develop an analytical model that is physically based and only uses measurable  
29 parameters, some of the required input values are not available at the global scale (e.g., carry  
30 over parameter ( $A$ ), interception storage capacity ( $S_{max}$ ), and plant available water ( $S_{u,max}$ )).  
31 Now with the current developments in remotely sensed data, new opportunities have arisen to  
32 overcome this data limitation. Therefore, in this study, we propose relations between the missing  
33 input parameters and remotely sensed data products, so the Gerrits' model can be tested at the  
34 global scale.

35 One of the input parameters is soil moisture storage. Recently, many studies (e.g., Chen et al.,  
36 2013; Donohue et al., 2010; Istanbuloglu et al., 2012; Milly and Dunne, 2002; Wang, 2012;  
37 Zhang et al., 2008) found that soil moisture storage change is a critical component in modelling  
38 the interannual water balance. Including soil water information into the Budyko framework was  
39 often difficult, because this information is not widely available. However, Gao et al. (2014)  
40 presented a new method where the available soil water (which is often linked to soil water

1 capacity) is derived from time series of rainfall and potential evaporation, plus a long-term  
 2 runoff coefficient. These input time series can be obtained locally (e.g., de Boer-Euser et al.  
 3 (2016)), but can also be derived from remotely sensed data as shown by Wang-Erlandsson et al.  
 4 (2016), allowing us to apply the method at the global scale and incorporate it in the Gerrits'  
 5 model.

6 Next to using the method of Gao et al (2014) to globally estimate the maximum soil water  
 7 storage ( $S_{u,max}$ ), we also tested a method to derive the interception storage capacity ( $S_{max}$ ) from  
 8 remotely sensed data. These two parameters are required to make a first order estimate of total  
 9 evaporation, and to partition this into interception evaporation and transpiration as well. The  
 10 outcome is compared to more complex land-surface-atmosphere models. Furthermore, the model  
 11 results will be related to the Budyko framework for a better understanding of the partitioning of  
 12 evaporation into transpiration and interception.

## 13 2. Methodology

14 Total evaporation ( $E$ ) may be partitioned as follows (Shuttleworth, 1993):

$$E = E_i + E_t + E_o + E_s \quad (2)$$

15 in which  $E_i$  is interception evaporation,  $E_t$  is transpiration,  $E_o$  is evaporation from water bodies  
 16 and  $E_s$  is evaporation from the soil, all with dimension [ $LT^{-1}$ ]. In this definition, interception is  
 17 the amount of evaporation from any wet surface including canopy, understory, forest floor, and  
 18 the top layer of the soil. Soil evaporation is defined as evaporation of the moisture in the soil that  
 19 is connected to the root zone (de Groen and Savenije, 2006) and therefore is different from  
 20 evaporation of the top layer of the soil (several millimeters of soil depth, which is here  
 21 considered as part of the interception evaporation). Hence interception evaporation is the fast  
 22 feedback of moisture to the atmosphere within a day from the rainfall event and soil evaporation  
 23 is evaporation from the non-superficial soil constrained by soil moisture storage in the root zone.  
 24 Like Gerrits et al. (2009), we assume that evaporation from soil moisture is negligible (or can be  
 25 combined with interception evaporation). Evaporation from water bodies is used for inland open  
 26 water, where interception evaporation and transpiration is zero. As a result, Eq. (2) becomes:

$$E = E_o \quad \text{for water bodies} \quad (3a)$$

$$E = E_i + E_t \quad \text{for land surface} \quad (3b)$$

27 where  $E_i$  is direct feedback from short term moisture storage on vegetation, ground, and top  
 28 layer, and  $E_t$  is evaporation from soil moisture storage in the root zone.

29 For modelling evaporation, it is important to consider that interception and transpiration have  
 30 different time scales (i.e. the stock divided by the evaporative flux) (Blyth and Harding, 2011).  
 31 With a stock of a few millimeters and the evaporative flux of a few millimeters per day,  
 32 interception has a time scale in the order of one day (Dolman and Gregory, 1992; Gerrits et al.,  
 33 2007, 2009; Savenije, 2004; Scott et al., 1995). In the case of transpiration, the stock amounts to  
 34 tens to hundreds of millimeteres and the evaporative flux to a few millimeters per day (Baird and  
 35 Wilby, 1999), resulting in a time scale in the order of month(s) (Gerrits et al., 2009). In Gerrits'

1 model, it is successively assumed that interception and transpiration can be modelled as  
2 threshold processes at the daily and monthly time scale, respectively. Rainfall characteristics are  
3 successively used to temporally upscale from daily to monthly, and from monthly to annual. A  
4 full description of the derivation and assumptions can be found in Gerrits et al. (2009). Here, we  
5 only summarize the relevant equations (Table 2) and not the complete derivation. Since we now  
6 test the model at the global scale, we do show how we estimated the required model parameters  
7 and the inputs used.

## 8 **2.1. Interception**

9 Gerrits' model considers evaporation from interception as a threshold process at the daily time  
10 scale (Eq. (4), Table 2). Daily interception ( $E_{i,d}$ ), then, is upscaled to monthly interception ( $E_{i,m}$ ,  
11 Eq. (5), Table 2) by considering the frequency distribution of rainfall on a rain day ( $\beta$ -parameter)  
12 and subsequently to annual interception ( $E_{i,a}$ , Eq. (6), Table 2) by considering the frequency  
13 distribution of rainfall in a rain month ( $\kappa_m$ -parameter) (see de Groen and Savenije (2006),  
14 Gerrits et al. (2009)). A rain day is defined as a day with more than  $0.1 \text{ mm day}^{-1}$  of rain and a  
15 rain month is a month with more than  $2 \text{ mm month}^{-1}$  of rain.

16 While Gerrits et al. (2009) assumed a constant interception threshold ( $D_{i,d} = 5 \text{ mm day}^{-1}$ ) for the  
17 studied locations, we here use a globally variable value based on the Leaf Area Index (LAI) from  
18 remote sensing data. The interception threshold ( $D_{i,d}$ ) is a daily average during the year and is  
19 either limited by the daily interception storage capacity  $S_{max}$  ( $\text{mm day}^{-1}$ ) or by the daily potential  
20 evaporation (Eq. (9), Table 2) and thus not seasonally variable. We can assume this because for  
21 most locations  $S_{max}$  is smaller than  $E_{p,d}$  even if we consider a daily varying potential  
22 evaporation. Additionally,  $S_{max}$  (based on LAI) could also be changed seasonally, however  
23 many studies show that the storage capacity is not changing significantly between the leafed and  
24 leafless period (e.g., Leyton et al., 1967; Dolman, 1987; Rutter et al., 1975). Especially, once  
25 interception is defined in a broad sense that it includes all evaporation from the canopy,  
26 understory, forest floor, and the top layer of the soil: leaves that are dropped from the canopy  
27 remain their interception capacity as they are on the forest floor in the leafless period.  
28 Furthermore, Gerrits et al (2010) showed with a Rutter-like model that interception is more  
29 sensitive to the rainfall pattern than by the storage capacity. This was confirmed by Miralles et  
30 al. (2010). Hence, in interception modelling, the value of the storage capacity is of minor  
31 concern, and its seasonality is incorporated in the temporal rainfall patterns.

32 The daily interception storage capacity should be seen as the maximum interception capacity  
33 within one day, including the (partly) emptying and filling of the storage between events per day,  
34 thus  $S_{max} = n \cdot C_{max}$ , where  $C_{max}$  [L] is the interception storage capacity specific for a land  
35 cover type. If there is only one rain event per day ( $n = 1 \text{ day}^{-1}$ ) (Gerrits et al., 2010),  $S_{max}$  [ $\text{LT}^{-1}$ ]  
36 equals  $C_{max}$  [L], as is often found in the literature. Despite proposing modifications for storms,  
37 which last more than one day (Pearce and Rowe, 1981), and multiple storms per rain day  
38 (Mulder, 1985), Miralles et al. (2010) and Pearce and Rowe (1981) both mentioned that  
39 accounting for  $n$  is rarely necessary. Pearce and Rowe (1981) mentioned that "In many climates,  
40 however, such adjustments will not be necessary, or small enough that they can be neglected". In

1 our interpretation, this is because the number of times the interception storage can be filled and  
2 completely emptied is limited once we assume a drying time of a couple of hours (e.g., 4), which  
3 is common (Wang-Erlandsson et al., 2014).

4 For  $n = 1$ , the interception storage capacity can be estimated from Von Hoyningen-Huene  
5 (1981), which is obtained for a series of crops based on the leaf area index (LAI) (de Jong and  
6 Jetten, 2007) (Eq. (10), Table 2). Since the storage capacity of the forest floor is not directly  
7 related to LAI, it could be said that the 0.935 mm in Eq. (10) is sort of the storage capacity of the  
8 forest floor. Since this equation was developed for crops, it is likely that it underestimates  
9 interception by forests with a denser understory and forest floor interception capacity.

## 10 2.2. Transpiration

11 Transpiration is considered as a threshold process at the monthly time scale ( $E_{t,m}$  (mm month<sup>-1</sup>),  
12 Eq. (7), Table 2) and successively is upscaled to annual transpiration ( $E_{t,a}$  (mm year<sup>-1</sup>), Eq. (8),  
13 Table 2) by considering the frequency distribution of the net monthly rainfall ( $P_{n,m} = P_m - E_{i,m}$ )  
14 expressed with the parameter  $\kappa_n$ . To estimate the monthly and annual transpiration, two  
15 parameters  $A$  and  $B$  are required.  $A$  is the initial soil moisture or carryover value (mm month<sup>-1</sup>)  
16 and  $B$  is dimensionless and described as Eq. (15), where the dimensionless  $\gamma$  is obtained by Eq.  
17 (16).

18 Gerrits et al. (2009) assumed a constant carry over value ( $A$ ) and used  $A = 0, 5, 15, 20$  mm  
19 month<sup>-1</sup>, depending on the location, to determine annual transpiration. Moreover, they  
20 considered  $\gamma$  to be constant ( $\gamma = 0.5$ ). In the current study, we determined these two parameters  
21 based on the maximum root zone storage capacity ( $S_{u,max}$ ). In Eq. (17)  $\Delta t_m$  equals 1 month and  
22  $S_b$  is estimated by  $aS_{u,max}$  (Eq. (18) in table 2), where  $a$  is 0.5-0.8 (de Groen, 2002;  
23 Shuttleworth, 1993). In this study, we assumed  $a$  to be 0.5 as this value is commonly used for  
24 many crops (Allen et al., 1998). Furthermore, we assumed that the monthly carry over  $A$  could  
25 be estimated by Eq. (18) and in this study, we assumed  $b = 0.2$  which gave the best global  
26 results for all land classes. In the sensitivity analysis both the sensitivity of  $a$  and  $b$  towards total  
27 evaporation will be investigated. To estimate  $A$  and  $\gamma$ , it is important to have a reliable database  
28 of  $S_{u,max}$ . For this purpose, we used the global estimation of  $S_{u,max}$  from Wang-Erlandsson et  
29 al. (2016).  $S_{u,max}$  is derived by the mass balance method using satellite based precipitation and  
30 evaporation (Wang-Erlandsson et al., 2016). Wang-Erlandsson et al. (2016) estimated the root  
31 zone storage capacity from the maximum soil moisture deficit, as the integral of the outgoing  
32 flux (i.e. evaporation which is the sum of transpiration, evaporation, interception, soil moisture  
33 evaporation, and open water evaporation) minus the incoming flux (i.e. precipitation and  
34 irrigation). In their study, the root zone storage capacity was defined as the total amount of water  
35 that plants can store to survive droughts. Note that this recent method (Gao et al., 2014) to  
36 estimate  $S_{u,max}$  does not require soil information, but only uses climatic data. It is assumed that  
37 ecosystems adjust their storage capacity to climatic demands irrespective of the soil properties.  
38 Under wet conditions, Gao's method appeared to perform better than soil-based methods. For  
39 (semi-)arid climates the difference between this method and soil-based methods appear to be  
40 small (de Boer-Euser et al., 2016).

1 Furthermore, Gerrits et al. (2009) estimated the average monthly transpiration threshold ( $D_{t,m}$ )  
2 as  $\frac{E_p - E_{i,a}}{n_a}$  (where  $n_a$  = number of months per year), which assumes that if there is little  
3 interception, plants can transpire at the same rate as a well-watered reference grass as calculated  
4 with the Penman-Monteith equation (University of East Anglia Climatic Research Unit, 2014).  
5 In reality, most plants encounter more resistance (crop resistance) than grass, hence we used Eq.  
6 (17), Table 2 (Fredlund et al., 2012) to convert potential evaporation of reference grass ( $E_p$ ) to  
7 potential transpiration of a certain crop depending on the LAI (i.e. the transpiration threshold  
8  $D_{t,m}$  [mm month<sup>-1</sup>]). Furthermore, similar to the daily interception threshold, we took a constant  
9  $D_{t,m}$ , which can be problematic in energy-constrained areas. However, in those areas often  
10 temperature and radiation follow a sinusoidal pattern without complex double seasonality as e.g.,  
11 occurs in the ITCZ. This implies that the overestimation of  $E_{t,m}$  in winter will be compensated  
12 (on the annual time scale) by the underestimation in summer time. By means of a sensitivity  
13 analysis the effect of a constant  $D_{t,m}$  will be investigated.

### 14 **3. Data**

15 For precipitation, we used the AgMERRA product from AgMIP climate forcing dataset (Ruane  
16 et al., 2015), which has a daily time scale and a spatial resolution of 0.25°×0.25°. The spatial  
17 coverage of AgMERRA is globally for the years 1980-2010. The AgMERRA product is  
18 available on the NASA Goddard Institute for Space Studies website  
19 (<http://data.giss.nasa.gov/impacts/agmipcf/agmerra/>).

20 Potential evaporation data (calculated by FAO-Penman–Monteith equation (Allen et al., 1998))  
21 were taken from Center for Environmental Data Archival website  
22 (<http://catalogue.ceda.ac.uk/uuid/4a6d071383976a5fb24b5b42e28cf28f>), produced by the  
23 Climatic Research Unit (CRU) at the University of East Anglia (University of East Anglia  
24 Climatic Research Unit, 2014). These data are at the monthly time scale over the period 1901-  
25 2013 and has a spatial resolution of 0.5°×0.5°. We used the data of 1980-2010 in consistent with  
26 precipitation dataset.

27 LAI data were obtained from Vegetation Remote Sensing & Climate Research  
28 (<http://sites.bu.edu/cliveg/datacodes/>) (Zhu et al., 2013). The spatial resolution of the data sets is  
29 1/12 degree, with 15-day composites (2 per month) for the period July 1981 to December 2011.

30 The data of  $S_{u,max}$  is prepared data by Wang-Erlandsson et al. (2016) and is based on the  
31 satellite-based precipitation and evaporation with 0.5°×0.5° resolution over the period 2003-  
32 2013. They used the USGS Climate Hazards Group InfraRed Precipitation with Stations  
33 (CHIRPS) precipitation data at 0.05° (Funk et al., 2014) and the ensemble mean of three datasets  
34 of evaporation including CSIRO MODIS Reflectance Scaling EvapoTranspiration (CMRSET) at  
35 0.05° (Guerschman et al., 2009), the Operational Simplified Surface Energy Balance (SSEBop)  
36 at 30" (Senay et al., 2013) and MODIS evapotranspiration (MOD16) at 0.05° (Mu et al., 2011).  
37 They calculated potential evaporation using the Penman-Monteith equation (Monteith, 1965).

### 38 **4. Model comparison and evaluation**

1 The model performance was evaluated by comparing our results at the global scale to global  
2 evaporation estimates from other studies. Most available products only provide total evaporation  
3 estimates and do not distinguish between interception and transpiration. Therefore, we chose to  
4 compare our interception and transpiration results to two land surface models: The Global Land  
5 Evaporation Amsterdam Model (GLEAM) (v3.0a) database (Martens et al., 2017; Miralles et al.,  
6 2011a) and Simple Terrestrial Evaporation to Atmosphere Model (STEAM) (Wang-Erlandsson  
7 et al., 2014, Wang-Erlandsson et al., 2016). GLEAM estimates different fluxes of evaporation  
8 including transpiration, interception, bare soil evaporation, snow sublimation, and open water  
9 evaporation. STEAM, on the other hand, estimates the different components of evaporation  
10 including transpiration, vegetation interception, floor interception, soil moisture evaporation, and  
11 open water evaporation. Thus for the comparison of interception, we used the sum of the canopy  
12 and floor interception and soil evaporation from STEAM and canopy interception and bare soil  
13 evaporation from GLEAM. Furthermore, STEAM includes an irrigation module (Wang-  
14 Erlandsson et al., 2014), while Miralles et al. (2011) mentioned that they did not include  
15 irrigation in GLEAM, but the assimilation of the soil moisture from satellite data would account  
16 for it as soil moisture adjusted to seasonal dynamics of any region. The total evaporation was  
17 also compared to LandFlux-EVAL products (Mueller et al., 2013). GLEAM database  
18 ([www.gleam.eu](http://www.gleam.eu)) is available for 1980-2014 with a resolution of  $0.25^\circ \times 0.25^\circ$  and STEAM model  
19 was performed for 2003-2013 with a resolution of  $1.5^\circ \times 1.5^\circ$ . LandFlux-EVAL data  
20 (<https://data.iac.ethz.ch/landflux/>) is available for 1989-2005. We compared Gerrits' model to  
21 other products based on the land cover to judge the performance of the model for different types  
22 of land cover. The global land cover map (Channan et al., 2014; Friedl et al., 2010) was obtained  
23 from <http://glcf.umd.edu/data/lc/>. We used root mean square error (*RMSE*) (Eq. 20), mean bias  
24 error (*MBE*) (Eq. 21) and relative error (*RE*) (Eq. 22) to evaluate the results.

$$\text{RMSE} = \sqrt{\frac{\sum_{i=1}^n (x_{iG} - x_{iM})^2}{n}} \quad (20)$$

$$\text{MBE} = \frac{\sum_{i=1}^n (x_{iG} - x_{iM})}{n} \quad (21)$$

$$\text{RE} = \frac{\bar{x}_G - \bar{x}_M}{\bar{x}_G} \times 100 \quad (22)$$

25 In these equations,  $x_{iM}$  is evaporation of the benchmark models to which Gerrits' model is  
26 compared for pixel  $i$ ,  $x_{iG}$  is evaporation from Gerrits' model for pixel  $i$ ,  $\bar{x}_G$  is the average  
27 evaporation of Gerrits' model,  $\bar{x}_M$  is the average evaporation of the benchmark models and  $n$  is  
28 the number of pixels of the evaporation map. Negative MBE and RE show the Gerrits' model  
29 underestimates evaporation and vice versa. As the spatial resolution of the products is different,  
30 we regridded all the products to the coarsest resolution ( $1.5^\circ \times 1.5^\circ$ ) for the comparison.  
31 Furthermore, the comparisons were shown for each land cover using the Taylor diagram (Taylor,  
32 2001). A Taylor diagram can provide a concise statistical summary of how the models are  
33 comparable to the reference data (observation or given model) in terms of their correlation,  
34 RMSE, and the ratio of their variances. In this paper, the reference data is Gerrits' model. Since  
35 the different models for different land cover types have been used in this study, which have  
36 different numerical values, the results are normalized by the reference data. It should be noted  
37 that the standard deviation of the reference data is normalized by itself and, therefore, it is

1 plotted at unit distance from the origin along the horizontal axis (Taylor, 2001). According to the  
2 Taylor diagram, when the points are close to reference data ('Ref' in Figures 2, 4 and 6), it  
3 shows that the RMSE is less and the correlation is higher and therefore, the models are in more  
4 reasonable agreement.

## 5 **5. Results and discussion**

### 6 **5.1. Total evaporation comparison**

7 Figure 1 shows the mean annual evaporation from Gerrits' model, Landflux-EVAL, STEAM and  
8 GLEAM data sets. In general, the spatial distribution of evaporation simulated by Gerrits' model  
9 is similar to that of the benchmark models. Figure 1a demonstrates that, as expected, the highest  
10 annual evaporation (sum of interception evaporation and transpiration) occurs in tropical  
11 evergreen broadleaf forests and the lowest rate occurs in the barren and sparsely vegetated desert  
12 regions. Total evaporation varies between almost zero in arid regions to more than 1500 mm  
13 year<sup>-1</sup> in the tropics.

14 As can be seen in Figure 1 there exist also large differences between STEAM, GLEAM, and  
15 Landflux-EVAL. Different precipitation products used in the models are likely the reason for the  
16 differences. As found by Gerrits et al. (2009), the model sensitivity to the number of rain days  
17 and rain months especially for the higher rates of precipitation can be a probable reason for the  
18 poor performance of a model especially for the forests with the highest amount of precipitation.  
19 In Sect. 5.5 we will elaborate on the sensitivity of these parameters on the global scale.

20 The contribution of mean annual evaporation per land cover type from Gerrits' model and other  
21 products, as well as RMSE, MBE and RE are shown in Table 3. Globally, mean annual  
22 evaporation estimated (for the overlapped pixels with 1.5°×1.5° resolution) by Gerrits' model,  
23 Landflux-EVAL, STEAM and GLEAM are 443, 469, 475 and 462 mm year<sup>-1</sup>, respectively. Our  
24 results are comparable to those of Haddeland et al. (2011), where the simulated global terrestrial  
25 evaporation ranges between 415 and 586 mm year<sup>-1</sup> for the period 1985–1999. Generally,  
26 Gerrits' model overestimates evaporation for most land cover types in comparison to Landflux-  
27 EVAL and GLEAM and underestimates in comparison to STEAM (see also MBE and RE).  
28 Since the number of pixels covered by each land use is different, RMSE, MBE, and RE cannot  
29 be comparable between land cover types. RMSE, MBE, and RE for each land cover type show  
30 that, generally, Gerrits' model is in a better agreement with Landflux and GLEAM than  
31 STEAM. The Taylor diagram for total evaporation, as estimated by Gerrits' model in  
32 comparison to Landflux-EVAL, STEAM and GLEAM for all data (No. 1 in Fig. 2) and for each  
33 land cover type (No.2 to No.11 in Fig. 2), also indicates that Gerrits' model is in better  
34 agreement with Landflux-EVAL and GLEAM than STEAM model, especially for evergreen  
35 broadleaf forest, shrublands, savannas, and croplands (see also Table 3).

### 36 **5.2. Annual interception comparison**

37 While Wang-Erlandsson et al. (2014; 2016) estimated canopy interception, floor interception,  
38 and soil evaporation separately, in the current study we assumed that these three components of  
39 evaporation can be lumped as interception evaporation. Figure 3 shows the mean annual



1 evaporation from interception at the global scale as estimated by Gerrits' model, STEAM, and  
2 GLEAM. In this figure, interception from STEAM is calculated by the sum of canopy  
3 interception, floor interception, and soil evaporation. Furthermore, interception from GLEAM is  
4 calculated as the sum of canopy interception and bare soil evaporation (GLEAM does not  
5 estimate floor interception). In general, the spatial distribution of Gerrits' simulated interception  
6 is partly similar to that of STEAM and GLEAM. In the tropics, with high amounts of annual  
7 precipitation and high storage capacities due to the dense vegetation (evergreen broadleaf forests  
8 and savannas), annual interception shows the highest values. Table 4 shows the average  
9 interception, RMSE, MBE and RE per land cover type. This table indicates that Gerrits' model  
10 underestimates interception in comparison to STEAM for all land cover types. Table 4 also  
11 shows that, in comparison to GLEAM, Gerrits' model overestimates interception for all land  
12 cover types, because in GLEAM floor interception has not been taken into account. Figure 4 also  
13 shows that Gerrits' model is in better agreement with STEAM (especially for grasslands and  
14 mixed forest) than GLEAM. The reason for an underestimated interception in comparison to  
15 STEAM could be the role of the understory. LAI does not account for understory, therefore  
16 maybe  $S_{max}$  should be larger than modeled with Eq. (10). However, there is almost no data  
17 available to estimate the interception storage capacity of the forest floor at the global scale.

### 18 **5.3. Annual transpiration comparison**

19 Figure 5 illustrates the mean annual transpiration as estimated by Gerrits' model, STEAM, and  
20 GLEAM. The spatial distribution is similar to the results of STEAM and GLEAM. Mean annual  
21 transpiration varies between 0 mm year<sup>-1</sup> for arid areas in the north of Africa (Sahara) to more  
22 than 1000 mm year<sup>-1</sup> in the tropics in South America. The results show that the highest annual  
23 transpiration occurs in evergreen broadleaf forests with the highest amount of precipitation and  
24 dense vegetation (see also Table 5). Figure 5c shows that GLEAM, in comparison to Gerrits'  
25 model, overestimates the transpiration in some regions and especially in the tropics in South  
26 America and Central Africa. Figure 5b also shows that STEAM is different from Gerrits' model  
27 over some regions like India, western China, and North America as well as in the tropics. Table  
28 5 (MBE and RE) also indicates that Gerrits' model underestimates transpiration in comparison to  
29 GLEAM and overestimates in comparison to STEAM. The Taylor diagram (Fig. 6) shows that  
30 the global annual transpiration of Gerrits' model is closer to that of GLEAM than STEAM.  
31 Representing that the Gerrits' model is in a more reasonable agreement to GLEAM for  
32 transpiration estimation.

33 Moreover, global transpiration ratio as estimated by Gerrits' model is 71% which is comparable  
34 to the ratio as estimated by other studies (e.g., 80% (Miralles et al., 2011b), 69% (Sutanto, 2015),  
35 65% (Good et al., 2015), 62% (Maxwell and Condon, 2016), 62% (Lian et al., 2018), 61%  
36 (Schlesinger and Jasechko, 2014), 57% (Wei et al., 2017), 52% (Choudhury and Digirolamo,  
37 1998), 48% (Dirmeyer et al., 2006) and 41% (Lawrence et al., 2007)). Additionally, Coenders-  
38 Gerrits et al. (2014) found that based on the model of Jasechko et al. (2013) the transpiration  
39 ratio changes between 35% and 80%, which is in line with our current findings.

### 40 **5.4. Analyzing the results through Budyko framework**

1 We evaluated the relation between the evaporation fluxes and the energy/water limitation in the  
 2 Budyko framework as provided by Miralles et al. (2016) and Good et al. (2017) to see how our  
 3 model can be related to the Budyko framework and how the energy and water limitations can be  
 4 interpreted by our model. Figure 7 shows the density plot of  $\frac{E}{P}$  versus  $\frac{E_p}{P}$  within the Budyko  
 5 framework. For calculating  $\frac{E}{P}$  and  $\frac{E_p}{P}$  for all models, precipitation and potential evaporation data  
 6 are the same as used in this study. This figure indicates that, while Gerrits' model does not  
 7 perform well in comparison to STEAM and GLEAM, it follows the framework in a reasonable  
 8 manner. Furthermore, the results are comparable to the results of Miralles et al. (2016) (see Fig.  
 9 11 in their paper). The partition of evaporation related to the land cover within the Budyko  
 10 framework is presented in Figure 8. According to this figure, interception, as estimated by  
 11 Gerrits' model, is closer to that of GLEAM rather than STEAM, but transpiration is close to both  
 12 models. For mean annual total evaporation, Gerrits' model is more similar to GLEAM than  
 13 STEAM for all land covers except for grasslands and shrublands. Moreover, the distribution of  $\frac{E_t}{P}$   
 14 is comparable to that of Good et al. (2017) (Figure 1.a in their paper). Their results showed a  
 15 unimodal  $\frac{E_t}{P}$  distribution indicating that both increasing and decreasing aridity will result in a  
 16 decline in the fraction of transpired rainfall by plants for growth and metabolism. This  
 17 distribution is also seen in Figure 9, where the plot is provided based on the average of  $\frac{E}{P}$  for each  
 18 aridity index ( $\frac{E_p}{P}$ ). This figure is also comparable to Figure 1.c in Good et al. (2017)'s paper.

## 19 5.5. Sensitivity analysis

20 In our sensitivity analysis we investigated the sensitivity of the three parameters that are related  
 21 to transpiration (constants  $a$  and  $b$ , and threshold  $D_{t,m}$ ), and the effect of the number of rain days  
 22 and rain months on the total evaporation calculation. All parameters were in- and decreased by  
 23 10%. The analysis shows that the model is not too sensitive to parameter  $a$ , where a  $\pm 10\%$   
 24 change in  $a$  leads to a minor  $\pm 0.4\%$  change in  $\frac{E}{P}$  (See Fig. 10.a). Thus, the model is insensitive to  
 25 changes in parameter  $a$ . Similar results were found for parameter  $b$ , where a  $\pm 10\%$  change in  $b$   
 26 resulted only in a  $\pm 3.5\%$  change in  $\frac{E}{P}$  (Fig. 10.b). Moreover, a  $\pm 10\%$  change in both  $n_{r,d}$  and  
 27  $n_{r,m}$  leads to a  $\pm 2.2$  change in  $\frac{E}{P}$  (Fig. 10.c and 10.d). The most sensitive parameter is  $D_{t,m}$ , where  
 28 a  $\pm 10\%$  change in  $D_{t,m}$  resulted in a  $\pm 4\%$  change in  $\frac{E}{P}$  (Fig. 10.e). In conclusion,  $D_{t,m}$  and  $b$  are  
 29 the most sensitive parameters for the estimation of  $\frac{E}{P}$ ; however, it seems that the sensitivity is not  
 30 that much different per land class. Except for grasslands and shrublands, which may arise from  
 31 the underestimation of interception in Gerrits' model for short vegetation. This underestimation  
 32 is obtained because the relation between  $S_{max}$  and LAI might not be valid for short vegetation.  
 33 This also might be due to the wide range of gridded points belong to grasslands and shrublands  
 34 as shown by the density plot of  $\frac{E}{P}$  versus  $\frac{E_p}{P}$  in Figure 11.

## 35 6. Conclusion

1 In the current study, we revised and applied a simple evaporation model proposed by Gerrits et  
2 al. (2009) at the global scale. Instead of locally calibrated model parameters we now only used  
3 parameters derived from remotely sensed data. Furthermore, we implemented in the Gerrits'  
4 model a new definition of the root zone storage capacity from Gao et al (2014).

5 Comparing our results for total evaporation to Landflux-EVAL estimates, shows that Gerrits'  
6 model is in good agreement with Landflux-EVAL. The highest mean annual evaporation rates  
7 are found in evergreen broadleaf forests (1367 mm year<sup>-1</sup>), deciduous broadleaf forests (796 mm  
8 year<sup>-1</sup>) and savannas (695 mm year<sup>-1</sup>) and the lowest ones are found in shrublands (203 mm year<sup>-1</sup>)  
9 and grasslands (275 mm year<sup>-1</sup>). Generally, Gerrits' model overestimates in comparison to  
10 Landflux-EVAL and GLEAM and underestimates in comparison to STEAM.

11 Gerrits' model underestimates interception in comparison to STEAM for all land covers. On the  
12 other hand, the model overestimates interception in comparison to GLEAM, since GLEAM does  
13 not include floor interception. Although we tried to correct for the different definitions of  
14 interception, the results may be biased. The relatively worse performance in forests ecosystems  
15 could be explained by the effect of the understory. This is not taken into account in Gerrits'  
16 model, while the understory can also intercept water. We could say that the constant value of  
17 0.935 mm in Eq. (10) reflects the forest floor interception storage capacity, but since this number  
18 was derived for crops, it is likely an underestimation. Therefore, a better estimation of  $S_{max}$  to  
19 account for forest floor interception is recommended.

20 Estimated transpiration by Gerrits' model is in reasonable agreement with GLEAM and  
21 STEAM. Gerrits' model underestimates transpiration in comparison to GLEAM (RE=-4%) and  
22 overestimates in comparison to STEAM (RE=+12%). The scatter plots showed that, in  
23 comparison to GLEAM and STEAM, Gerrits' model performs well for all land cover types.  
24 Moreover, the transpiration ratio corresponded well in comparison to those of GLEAM and  
25 STEAM. The results also showed that the global transpiration ratio estimated by Gerrits' model  
26 (71%) is approximately comparable to the other studies.

27 Our results are also related to the Budyko framework and we found similar to Good et al. (2017)  
28 that the distribution of  $\frac{E_t}{P}$  is unimodal, indicating that both increasing and decreasing aridity will  
29 result in decline in the fraction of transpired precipitation by plants for growth and metabolism.

30 By comparing all products, we found that, in general, there are considerable differences between  
31 STEAM, GLEAM, and Landflux-EVAL. The most convincing reason for this discrepancy lies in  
32 the different products for precipitation (and other global data sets), which have been used for the  
33 different models. The Gerrits' model is sensitive to the number of rain days and months  
34 especially for the higher rates of precipitation. Nonetheless, our sensitivity analysis of  
35 parameters  $a$  and  $b$  and  $n_{r,d}$ ,  $n_{r,m}$  and  $D_{t,m}$  shows that  $D_{t,m}$  and  $b$  are the most sensitive  
36 parameters for the estimation of  $\frac{E}{P}$ .

37 Generally, it should be mentioned that the underlying reasoning of the Gerrits' model is to  
38 recognize the characteristic time scales of the different evaporation processes (i.e. interception  
39 daily and transpiration monthly). In Gerrits et al. (2009) (and in the current paper as well), this

1 has been done by taking yearly averages for the interception ( $D_{i,d}$ , mm day<sup>-1</sup>) and transpiration  
2 threshold ( $D_{t,m}$ , mm month<sup>-1</sup>) in combination with the temporal distribution functions for daily  
3 and monthly (net) rainfall. Hence, the seasonality is incorporated in the temporal rainfall  
4 patterns, and not in the evaporation thresholds. This is a limitation of the currently used approach  
5 and could be the focus of a new study by investigating how seasonal fluctuating thresholds  
6 (based on LAI and/or a simple cosine function) would affect the results. This could be a  
7 significant methodological improvement of the Gerrits' model, but will have mathematical  
8 implications on the analytical model derivation. It will improve the monthly evaporation  
9 estimates, but we expect that the consequences at the annual time scale (which is the focus of the  
10 current paper) will be less severe. The strength of the Gerrits' model is that, in comparison to  
11 other models, it is very simple and in spite of its simplicity, the Gerrits' model performs quite  
12 well.

### 13 **Author contribution**

14 Ameneh Mianabadi and Miriam Coenders-Gerrits implemented the model on the global scale  
15 and analyzed the data. Pooya Shirazi helped with the code programming. Ameneh Mianabadi  
16 and Miriam Coenders-Gerrits prepared the manuscript with contribution from all co-authors.

### 17 **Acknowledgment**

18 This research was partly funded by NWO Earth and Life Sciences (ALW), Veni-project  
19 863.15.022, the Netherlands. Furthermore, we would like to thank Iran's Ministry of Science,  
20 Research and Technology for supporting this research and the mobility fellowship. We also  
21 would like to thank Jie Zhou, Lan Wang-Erlandsson, Kamran Davary, Shervan Gharari and  
22 Hubert Savenije for their kind helps and comments.

### 23 **Competing interests**

24 The authors declare that they have no conflict of interest.

### 25 **References**

- 26 Allen, R., Pereira, L., Raes, D. and Smith, M.: Crop evapotranspiration: Guidelines for  
27 computing crop water requirements, FAO Irrig. Drain. Pap. 56. FAO, Rome, Italy, 300 p, 1998.
- 28 Arora, V. K.: The use of the aridity index to assess climate change effect on annual runoff, J.  
29 Hydrol., 265(1–4), 164–177, doi:10.1016/S0022-1694(02)00101-4, 2002.
- 30 Baird, A. J. and Wilby, R. L.: Eco-hydrology: Plants and Water in Terrestrial and Aquatic  
31 Environments, Routledge, London., 1999.
- 32 Blyth, E. and Harding, R. J.: Methods to separate observed global evapotranspiration into the  
33 interception, transpiration and soil surface evaporation components, Hydrol. Process., 25, 4063–  
34 4068, doi:10.1002/hyp.8409, 2011.
- 35 de Boer-Euser, T., McMillan, H. K., Hrachowitz, M., Winsemius, H. C. and Savenije, H. H. G.:  
36 Influence of soil and climate on root zone storage capacity, Water Resour. Res., 17(2014),

1 accepted, doi:10.1002/2015WR018115, 2016.

2 Channan, S., Collins, K. and Emanuel, W. R.: Global mosaics of the standard MODIS land cover  
3 type data, College Park, Maryland, USA., 2014.

4 Chen, X., Alimohammadi, N. and Wang, D.: Modeling interannual variability of seasonal  
5 evaporation and storage change based on the extended Budyko framework, *Water Resour. Res.*,  
6 49(9), 6067–6078, doi:10.1002/wrcr.20493, 2013.

7 Choudhury, B.: Evaluation of an empirical equation for annual evaporation using field  
8 observations and results from a biophysical model, *J. Hydrol.*, 216(1–2), 99–110,  
9 doi:10.1016/S0022-1694(98)00293-5, 1999.

10 Choudhury, B. and Digirolamo, N. E.: A biophysical process-based estimate of global land  
11 surface evaporation using satellite and ancillary data I. Model description and comparison with  
12 observations, *J. Hydrol.*, 205, 164–185, 1998.

13 Coenders-Gerrits, A. M. J., van der Ent, R. J., Bogaard, T. A., Wang-Erlandson, L., Hrachowitz,  
14 M. and Savenije, H. H. G.: Uncertainties in transpiration estimates, *Nature*, 506, E1–E2,  
15 doi:10.1038/nature12925, 2014.

16 Dirmeyer, P. A., Gao, X., Zha, M., Guo, Z., Oki, T. and Hanasaki, N.: GSWP-2: Multimodel  
17 analysis and implications for our perception of the land surface, *Bull. Am. Meteorol. Soc.*, 87,  
18 1381–1397, doi:10.1175/BAMS-87-10-1381, 2006.

19 Dolman, a J. and Gregory, D.: The Parametrization of Rainfall Interception In GCMs, *Q. J. R.*  
20 *Meteorol. Soc.*, 118(505), 455–467, doi:10.1002/qj.49712051713, 1992.

21 Donohue, R. J., Roderick, M. L. and Mcvicar, T. R.: On the importance of including vegetation  
22 dynamics in Budyko ’ s hydrological model, *Hydrol. Earth Syst. Sci.*, 11, 983–995, 2007.

23 Donohue, R. J., Roderick, M. L. and McVicar, T. R.: Can dynamic vegetation information  
24 improve the accuracy of Budyko’s hydrological model?, *J. Hydrol.*, 390(1–2), 23–34,  
25 doi:10.1016/j.jhydrol.2010.06.025, 2010.

26 Fredlund, D. G., Rahardjo, H. and Fredlund, M. D.: *Unsaturated Soil Mechanics in Engineering*  
27 *Practice*, John Wiley & Sons, Ltd., 2012.

28 Friedl, M. A., Sulla-Menashe, D., Tan, B., Schneider, A., Ramankutty, N., Sibley, A. and Huang,  
29 X.: MODIS Collection 5 global land cover: Algorithm refinements and characterization of new  
30 datasets, 2001-2012, Collection 5.1 IGBP Land Cover, Boston, MA, USA., 2010.

31 Gao, H., Hrachowitz, M., Schymanski, S. J., Fenicia, F., Sriwongsitanon, N. and Savenije, H. H.  
32 G.: Climate controls how ecosystems size the root zone storage capacity at catchment scale,  
33 *Geophys. Res. Lett.*, 41(22), 7916–7923, doi:10.1002/2014GL061668, 2014.

34 Gerrits, A. M. J., Savenije, H. H. G., Hoffmann, L. and Pfister, L.: New technique to measure  
35 forest floor interception – an application in a beech forest in Luxembourg, *Hydrol. Earth Syst.*  
36 *Sci.*, 11(2), 695–701, doi:10.5194/hess-11-695-2007, 2007.

37 Gerrits, A. M. J., Savenije, H. H. G., Veling, E. J. M. and Pfister, L.: Analytical derivation of the  
38 Budyko curve based on rainfall characteristics and a simple evaporation model, *Water Resour.*  
39 *Res.*, 45, W04403, doi:10.1029/2008WR007308, 2009.

40 Gerrits, A. M. J., Pfister, L. and Savenije, H. H. G.: Spatial and temporal variability of canopy  
41 and forest floor interception in a beech forest, *Hydrol. Process.*, 24(21), 3011–3025,

1 doi:10.1002/hyp.7712, 2010.

2 Good, S. P., Noone, D. and Bowen, G.: Hydrologic connectivity constrains partitioning of global  
3 terrestrial water fluxes, *Science* (80-. ), 349(6244), 175–177, 2015.

4 Good, S. P., Moore, G. W. and Miralles, D. G.: A mesic maximum in biological water use  
5 demarcates biome sensitivity to aridity shifts, *Nat. Ecol. Evol.*, 1(12), 1883–1888,  
6 doi:10.1038/s41559-017-0371-8, 2017.

7 de Groen, M. M.: Modelling interception and transpiration at monthly time steps : introducing  
8 daily variability through Markov chains. [online] Available from:  
9 <https://books.google.com/books?id=-birGVG44nkC&pgis=1>, 2002.

10 de Groen, M. M. and Savenije, H. H. G.: A monthly interception equation based on the statistical  
11 characteristics of daily rainfall, *Water Resour. Res.*, 42(12), W12417,  
12 doi:10.1029/2006WR005013, 2006.

13 Guerschman, J. P., Van Dijk, A. I. J. M., Mattersdorf, G., Beringer, J., Hutley, L. B., Leuning,  
14 R., Pipunic, R. C. and Sherman, B. S.: Scaling of potential evapotranspiration with MODIS data  
15 reproduces flux observations and catchment water balance observations across Australia, *J.*  
16 *Hydrol.*, 369(1–2), 107–119, doi:10.1016/j.jhydrol.2009.02.013, 2009.

17 Haddeland, I., Clark, D. B., Franssen, W., Ludwig, F., Voß, F., Arnell, N. W., Bertrand, N., Best,  
18 M., Folwell, S., Gerten, D., Gomes, S., Gosling, S. N., Hagemann, S., Hanasaki, N., Harding, R.,  
19 Heinke, J., Kabat, P., Koirala, S., Oki, T., Polcher, J., Stacke, T., Viterbo, P., Weedon, G. P. and  
20 Yeh, P.: Multimodel Estimate of the Global Terrestrial Water Balance : Setup and First Results,  
21 *J. Hydrometeorol.*, 12, 869–884, doi:10.1175/2011JHM1324.1, 2011.

22 Von Hoyningen-Huene, J.: Die Interzeption des Niederschlags in Landwirtschaftlichen  
23 Pflanzenbeständen, *Arbeitsbericht Dtsch. Verband für Wasserwirtschaft und Kult.*  
24 (Braunschweig DVWK), 1981.

25 Istanbuluoglu, E., Wang, T., Wright, O. M. and Lenters, J. D.: Interpretation of hydrologic  
26 trends from a water balance perspective: The role of groundwater storage in the Budyko  
27 hypothesis, *Water Resour. Res.*, 48(3), W00H16, doi:10.1029/2010WR010100, 2012.

28 Jasechko, S., Sharp, Z. D., Gibson, J. J., Birks, S. J., Yi, Y. and Fawcett, P. J.: Terrestrial water  
29 fluxes dominated by transpiration, *Nature*, 496(7445), 347–350, doi:10.1038/nature11983, 2013.

30 de Jong, S. M. and Jetten, V. G.: Estimating spatial patterns of rainfall interception from  
31 remotely sensed vegetation indices and spectral mixture analysis, *Int. J. Geogr. Inf. Sci.*, 21(5),  
32 529–545, doi:10.1080/13658810601064884, 2007.

33 Lawrence, D. M., Thornton, P. E., Oleson, K. W. and Bonan, G. B.: The Partitioning of  
34 Evapotranspiration into Transpiration , Soil Evaporation , and Canopy Evaporation in a GCM :  
35 Impacts on Land – Atmosphere Interaction, *J. Hydrometeorol.*, 8, 862–880,  
36 doi:10.1175/JHM596.1, 2007.

37 Lian, X., Piao, S., Huntingford, C., Li, Y., Zeng, Z., Wang, X., Ciais, P., Mcvicar, T. R., Peng,  
38 S., Ottlé, C., Yang, H., Yang, Y., Zhang, Y. and Wang, T.: CMIP5 models constrained by  
39 observations, *Nat. Clim. Chang.*, 8, 640–646, doi:10.1038/s41558-018-0207-9, 2018.

40 Martens, B., Miralles, D. G., Lievens, H., Van Der Schalie, R., De Jeu, R. A. M., Fernández-  
41 Prieto, D., Beck, H. E., Dorigo, W. A. and Verhoest, N. E. C.: GLEAM v3 : satellite-based land  
42 evaporation and root-zone soil moisture, *Geosci. Model Dev.*, 10, 1903–1925, doi:10.5194/gmd-

1 10-1903-2017, 2017.

2 Maxwell, R. M. and Condon, L. E.: Connections between groundwater flow and transpiration  
3 partitioning, *Science* (80-. ), 353(6297), 377–380, 2016.

4 Milly, P. C. D.: An analytic solution of the stochastic storage problem applicable to soil water,  
5 *Water Resour. Res.*, 29(11), 3755–3758, doi:10.1029/93WR01934, 1993.

6 Milly, P. C. D.: Climate, soil water storage, and the average annual water balance, *Water Resour.*  
7 *Res.*, 30(7), 2143–2156, doi:10.1029/94WR00586, 1994.

8 Milly, P. C. D. and Dunne, K. a.: Macroscale water fluxes 2. Water and energy supply control of  
9 their interannual variability, *Water Resour. Res.*, 38(10), 24-1-24-9,  
10 doi:10.1029/2001WR000760, 2002.

11 Miralles, D. G., Gash, J. H., Holmes, T. R. H., De Jeu, R. A. M. and Dolman, A. J.: Global  
12 canopy interception from satellite observations, *J. Geophys. Res. Atmos.*, 115(16), 1–8,  
13 doi:10.1029/2009JD013530, 2010.

14 Miralles, D. G., Holmes, T. R. H., De Jeu, R. A. M., Gash, J. H., Meesters, A. G. C. A. and  
15 Dolman, A. J.: Global land-surface evaporation estimated from satellite-based observations,  
16 *Hydrol. Earth Syst. Sci.*, 15(2), 453–469, doi:10.5194/hess-15-453-2011, 2011a.

17 Miralles, D. G., De Jeu, R. A. M., Gash, J. H., Holmes, T. R. H. and Dolman, A. J.: Magnitude  
18 and variability of land evaporation and its components at the global scale, *Hydrol. Earth Syst.*  
19 *Sci.*, 15, 967–981, doi:10.5194/hess-15-967-2011, 2011b.

20 Miralles, D. G., Jiménez, C., Jung, M., Michel, D., Ershadi, A., McCabe, M. F., Hirschi, M.,  
21 Martens, B., Dolman, A. J., Fisher, J. B., Mu, Q., Seneviratne, S. I., Wood, E. F. and Fernández-  
22 Prieto, D.: The WACMOS-ET project - Part 2: Evaluation of global terrestrial evaporation data  
23 sets, *Hydrol. Earth Syst. Sci.*, 20(2), 823–842, doi:10.5194/hess-20-823-2016, 2016.

24 Mu, Q., Zhao, M. and Running, S. W.: Improvements to a MODIS global terrestrial  
25 evapotranspiration algorithm, *Remote Sens. Environ.*, 115(8), 1781–1800,  
26 doi:10.1016/j.rse.2011.02.019, 2011.

27 Mueller, B., Hirschi, M., Jimenez, C., Ciais, P., Dirmeyer, P. A., Dolman, A. J., Fisher, J. B.,  
28 Jung, M., Ludwig, F., Maignan, F., Miralles, D. G., McCabe, M. F., Reichstein, M., Sheffield, J.,  
29 Wang, K., Wood, E. F., Zhang, Y. and Seneviratne, S. I.: Benchmark products for land  
30 evapotranspiration: LandFlux-EVAL multi-data set synthesis, *Hydrol. Earth Syst. Sci.*, 17(10),  
31 3707–3720, doi:10.5194/hess-17-3707-2013, 2013.

32 Mulder, J. P. M.: Simulating Interception Loss Using Standard Meteorological Data, in *The*  
33 *Forest-Atmosphere Interaction*, edited by B. A. Hutchison and B. B. Hicks, pp. 177–196., 1985.

34 Pearce, A. J. and Rowe, L. K.: Rainfall interception in a multi-storied, evergreen mixed forest:  
35 estimates using Gash’s analytical model, *J. Hydrol.*, 49, 341–353, doi:10.1016/S0022-  
36 1694(81)80018-2, 1981.

37 Porporato, A., Daly, E. and Rodriguez-Iturbe, I.: Soil water balance and ecosystem response to  
38 climate change, *Am. Nat.*, 164(5), 625–632, doi:10.1086/521238, 2004.

39 Ruane, A. C., Goldberg, R. and Chryssanthacopoulos, J.: Climate forcing datasets for  
40 agricultural modeling: Merged products for gap-filling and historical climate series estimation,  
41 *Agric. For. Meteorol.*, 200, 233–248, doi:10.1016/j.agrformet.2014.09.016, 2015.

1 Savenije, H. H. G.: The importance of interception and why we should delete the term  
2 evapotranspiration from our vocabulary, *Hydrol. Process.*, 18(8), 1507–1511,  
3 doi:10.1002/hyp.5563, 2004.

4 Schlesinger, W. H. and Jasechko, S.: Transpiration in the global water cycle, *Agric. For.  
5 Meteorol.*, 189–190, 115–117, doi:10.1016/j.agrformet.2014.01.011, 2014.

6 Scott, R., Koster, R. D., Entekhabi, D. and Suarez, M. J.: Effect of a Canopy Interception  
7 Reservoir on Hydrological Persistence in a General Circulation Model, *J. Clim.*, 8(7), 1917–  
8 1922, doi:10.1175/1520-0442(1995)008<1917:EOACIR>2.0.CO;2, 1995.

9 Senay, G. B., Bohms, S., Singh, R. K., Gowda, P. H., Velpuri, N. M., Alemu, H. and Verdin, J.  
10 P.: Operational Evapotranspiration Mapping Using Remote Sensing and Weather Datasets: A  
11 New Parameterization for the SSEB Approach, *J. Am. Water Resour. Assoc.*, 49(3), 577–591,  
12 doi:10.1111/jawr.12057, 2013.

13 Shuttleworth, W. J.: Evaporation, in *Handbook of Hydrology*, p. 4.1-4.53, McGraw-Hill, New  
14 York., 1993.

15 Sutanto, S. J.: Global transpiration fraction derived from water isotopologue datasets, *J. Tek.  
16 Hidraul.*, 6(2), 131–146, 2015.

17 Taylor, K. E.: Summarizing multiple aspects of model performance in a single diagram, *J.  
18 Geophys. Res.*, 106(D7), 7183–7192, 2001.

19 University of East Anglia Climatic Research Unit, Harris, I. C. and Jones, P. D.: CRU TS3.22:  
20 Climatic Research Unit (CRU) Time-Series (TS) Version 3.22 of High Resolution Gridded Data  
21 of Month-by-month Variation in Climate (Jan. 1901- Dec. 2013), NCAS Br. Atmos. Data Cent.,  
22 24 Septemb, doi:10.5285/18BE23F8-D252-482D-8AF9-5D6A2D40990C, 2014.

23 Wang-Erlandsson, L., Van Der Ent, R. J., Gordon, L. J. and Savenije, H. H. G.: Contrasting roles  
24 of interception and transpiration in the hydrological cycle - Part 1: Temporal characteristics over  
25 land, *Earth Syst. Dyn.*, 5(2), 441–469, doi:10.5194/esd-5-441-2014, 2014.

26 Wang-Erlandsson, L., Bastiaanssen, W. G. M., Gao, H., Jägermeyr, J., Senay, G. B., van Dijk,  
27 A. I. J. M., Guerschman, J. P., Keys, P. W., Gordon, L. J. and Savenije, H. H. G.: Global root  
28 zone storage capacity from satellite-based evaporation, *Hydrol. Earth Syst. Sci. Discuss.*,  
29 (December), 1–49, doi:10.5194/hess-2015-533, 2016.

30 Wang, D.: Evaluating interannual water storage changes at watersheds in Illinois based on long-  
31 term soil moisture and groundwater level data, *Water Resour. Res.*, 48(3),  
32 doi:10.1029/2011WR010759, 2012.

33 Wei, Z., Yoshimura, K., Wang, L., Miralles, D., Jasechko, S. and Lee, X.: Revisiting the  
34 contribution of transpiration to global terrestrial evapotranspiration, *Am. Geophys. Union*,  
35 doi:10.1002/2016GL072235, 2017.

36 Yang, D., Sun, F., Liu, Z., Cong, Z. and Lei, Z.: Interpreting the complementary relationship in  
37 non-humid environments based on the Budyko and Penman hypotheses, *Geophys. Res. Lett.*,  
38 33(18), 1–5, doi:10.1029/2006GL027657, 2006.

39 Yang, H., Yang, D., Lei, Z. and Sun, F.: New analytical derivation of the mean annual water-  
40 energy balance equation, *Water Resour. Res.*, 44(3), W03410, doi:10.1029/2007WR006135,  
41 2008.



1 Zhang, L., Dawes, W. R. and Walker, G. R.: Response of Mean Annual Evapotranspiration to  
2 Vegetation changes at Catchment Scale, *Water Resour.*, 37(3), 701–708, 2001.

3 Zhang, L., Hickel, K., Dawes, W. R., Chiew, F. H. S., Western, A. W. and Briggs, P. R.: A  
4 rational function approach for estimating mean annual evapotranspiration, *Water Resour. Res.*,  
5 40(2), WR002710, doi:10.1029/2003WR002710, 2004.

6 Zhang, L., Potter, N., Hickel, K., Zhang, Y. and Shao, Q.: Water balance modeling over variable  
7 time scales based on the Budyko framework – Model development and testing, *J. Hydrol.*,  
8 360(1–4), 117–131, doi:10.1016/j.jhydrol.2008.07.021, 2008.

9 Zhu, Z., Bi, J., Pan, Y., Ganguly, S., Anav, A., Xu, L., Samanta, A., Piao, S., Nemani, R. R. and  
10 Myneni, R. B.: Global data sets of vegetation leaf area index (LAI)3g and fraction of  
11 photosynthetically active radiation (FPAR)3g derived from global inventory modeling and  
12 mapping studies (GIMMS) normalized difference vegetation index (NDVI3G) for the period  
13 1981 to 2, *Remote Sens.*, 5(2), 927–948, doi:10.3390/rs5020927, 2013.

14

1 **Table 1-** Budyko equations developed by different researchers.

Equation	Reference
$\frac{E_a}{P_a} = 1 - \exp(-\phi)$	Schreiber [1904]
$\frac{E_a}{P_a} = \phi \tanh\left(\frac{1}{\phi}\right)$	Ol'dekop [1911]
$\frac{E_a}{P_a} = \frac{1}{\sqrt{0.9 + \left(\frac{1}{\phi}\right)^2}}$	Turc [1954]
$\frac{E_a}{P_a} = \frac{1}{\sqrt{1 + \left(\frac{1}{\phi}\right)^2}}$	Pike [1964]
$\frac{E_a}{P_a} = \left[\phi \tanh\left(\frac{1}{\phi}\right) (1 - \exp(-\phi))\right]^{1/2}$	Budyko [1974]

2

1 **Table 2-** Summary of the interception and transpiration equations of Gerrits' model (Gerrits et al., 2009)

Equation	Equation number	Description
$E_{i,d} = \min(D_{i,d}, P_d)$	(4)	$E_{i,d}$ : daily interception (mm day <sup>-1</sup> ), $P_d$ : daily precipitation (mm day <sup>-1</sup> ), $D_{i,d}$ : the daily interception threshold (mm day <sup>-1</sup> )
$E_{i,m} = P_m(1 - \exp(-\phi_{i,m}))$	(5)	$E_{i,m}$ : monthly interception (mm month <sup>-1</sup> ), $P_m$ : monthly rainfall (mm month <sup>-1</sup> ), $\phi_{i,m}$ : a sort of aridity index for interception at monthly scale
$E_{i,a} = P_a(1 - 2\phi_{i,a}K_0(2\sqrt{\phi_{i,a}}) - 2\sqrt{\phi_{i,a}}K_1(2\sqrt{\phi_{i,a}}))$	(6)	$E_{i,a}$ : annual interception (mm year <sup>-1</sup> ), $P_a$ : annual rainfall (mm year <sup>-1</sup> ), $\phi_{i,a}$ : a sort of aridity index for interception at annual scale, $K_0$ and $K_1$ : the Bessel function of the first and second order, respectively
$E_{t,m} = \min(A + B(P_m - E_{i,m}), D_{t,m})$	(7)	$E_{t,m}$ : monthly transpiration (mm month <sup>-1</sup> ), $A$ : carry-over parameter (mm month <sup>-1</sup> ), $D_{t,m}$ : the transpiration threshold (mm month <sup>-1</sup> ), $B$ : slope of relation between monthly effective rainfall and monthly transpiration
$A = bS_{u,max}$	(8)	$b$ : constant coefficient, $S_{u,max}$ : the maximum root zone storage capacity
$E_{t,a} = 2BP_a(\phi_{i,a}K_0(2\sqrt{\phi_{i,a}}) + \sqrt{\phi_{i,a}}K_1(2\sqrt{\phi_{i,a}}))$ $\left(\frac{A}{\kappa_n B} + 1 - \exp(-\phi_{t,a})\left(\frac{A}{\kappa_n B} + 1 + \phi_{t,a} - \frac{\phi_{t,a}}{B}\right)\right)$	(9)	$E_{t,a}$ : annual transpiration (mm year <sup>-1</sup> ), $\phi_{t,a}$ : an aridity index
$D_{i,d} = \min(S_{max}, E_{p,d})$	(10)	$S_{max}$ : the daily interception storage capacity (mm day <sup>-1</sup> ) $E_{p,d}$ : the daily potential evaporation, $E_{p,a}$ : annual potential evaporation (mm year <sup>-1</sup> )
$S_{max} \approx C_{max} = 0.935 + 0.498LAI - 0.00575LAI^2$	(11)	LAI: Leaf Area Index derived from remote sensing images
$\phi_{i,m} = \frac{D_{i,d}}{\beta}$	(12)	$\beta$ : scaling factor
$\beta = \frac{P_m}{E(n_{r,d} n_m)}$	(13)	$E(n_{r,d} n_m)$ : the expected number of rain days per month, $n_{r,d}$ : the number of rain days per month, $n_m$ : the number of days per month
$\phi_{i,a} = \frac{n_{r,d}D_{i,d}}{\kappa_m}$	(14)	$\kappa_m$ : scaling factor for monthly rainfall
$\kappa_m = \frac{P_a}{E(n_{r,m} n_a)}$	(15)	$E(n_{r,m} n_a)$ : the expected number of rain months per year, $n_{r,m}$ : the number of rain months per year, $n_a$ : the number of months per year
$B = 1 - \gamma + \gamma \exp(-\frac{1}{\gamma})$	(16)	$\gamma$ : time scale for transpiration
$\gamma = \frac{S_b}{D_{t,m}\Delta t_m}$	(17)	$S_b$ : the moisture content below which transpiration is restricted (mm).
$S_b = aS_{u,max}$	(18)	$a$ : constant coefficient
$D_{t,m} = 0$ for $LAI < 0.1$ $D_{t,m} = \frac{E_p}{n_a}(-0.21 + 0.7LAI^{0.5})$ for $0.1 \leq LAI < 2.7$ $D_{t,m} = \frac{E_p}{n_a}$ for $LAI \geq 2.7$	(19)	$E_p$ : annual potential evaporation (for open water) (mm year <sup>-1</sup> )
$\phi_{t,a} = \frac{D_{t,m}}{\kappa_n}$	(20)	$\kappa_n$ : scaling factor for monthly net rainfall
$\kappa_n = \frac{P_{n,a}}{E(n_{nr,m} n_a)} = \frac{P_a - E_{i,a}}{E(n_{nr,m} n_a)}$	(21)	$P_{n,a}$ : annual net precipitation, $E(n_{nr,m} n_a)$ : the expected number of net rain months per year

**Table 3-** Comparison of mean annual evaporation estimated by Gerrits’ model to Landflux-EVAL, STEAM and GLEAM through Average, RMSE, MBE and RE per land cover type. Negative MBE and RE show the Gerrits’ model underestimates evaporation and vice versa. Average, RMSE and MBE are in mm year<sup>-1</sup> and RE is in %.

Land cover	area	Gerrits	Landflux-EVAL				STEAM				GLEAM			
	1000 km <sup>2</sup>	Avg.	Avg.	RMSE	MBE	RE	Avg.	RMSE	MBE	RE	Avg.	RMSE	MBE	RE
Evergreen needleleaf forest	5563	430	387	122	+43	+10	467	150	-37	-9	457	127	-27	-6
Evergreen broadleaf forest	11778	1367	1177	266	+190	+14	1129	345	+238	+17	1244	225	+123	+9
Deciduous needleleaf forest	2498	338	298	73	+40	+12	336	65	+2	+1	336	73	+1	0
Deciduous broadleaf forest	1106	796	736	138	+61	+8	840	215	-44	-6	660	197	+136	+17
Mixed forest	13470	563	487	136	+76	+13	545	137	+18	+3	527	131	+35	+6
Shrublands <sup>1</sup>	29542	203	259	96	-57	-28	262	123	-59	-29	253	91	-51	-25
Savannas <sup>2</sup>	18846	695	739	148	-44	-6	737	186	-42	-6	705	154	-10	-1
Grasslands	21844	275	365	130	-91	-33	373	164	-98	-36	349	135	-75	-27
Croplands	12417	488	535	124	-47	-10	583	209	-95	-20	486	118	+2	0
Croplands and natural vegetation mosaic	5782	687	696	157	-9	-1	702	175	-15	-2	663	158	+24	+3
Global <sup>3</sup>	-	443	469	-	-	-6	475	-	-	-7	462	-	-	-4

<sup>1</sup>including open and closed shrublands. <sup>2</sup>including woody savannas and savannas. <sup>3</sup>for overlapped pixels with 1.5°×1.5° resolution.

**Table 4-** Comparison of interception estimated by Gerrits’ model to STEAM and GLEAM through Average, RMSE, MBE and RE per land cover type. Negative MBE and RE show the Gerrits’ model underestimates evaporation and vice versa. Average, RMSE and MBE are in mm year<sup>-1</sup> and RE is in %.

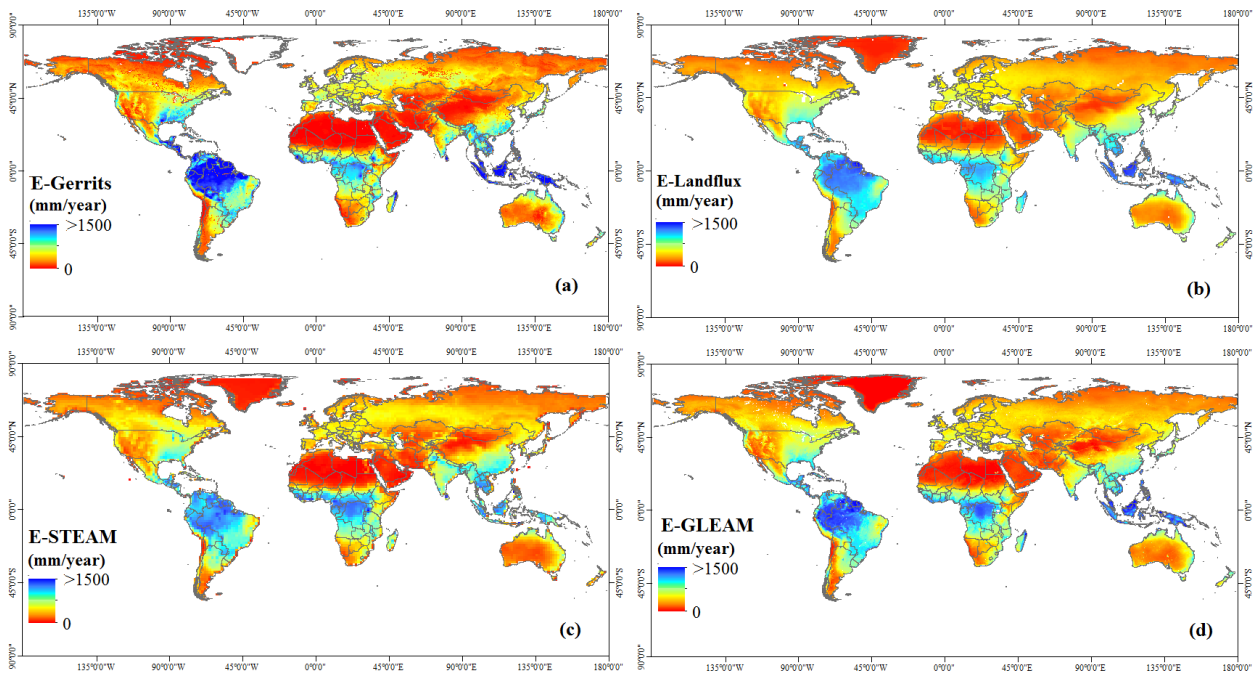
Land cover	Area	Gerrits	STEAM			GLEAM				
	1000 km <sup>2</sup>	Avg.	Avg.	RMSE	MBE	RE	Avg.	RMSE	MBE	RE
Evergreen needleleaf forest	5563	145	204	70	-58	-40	127	58	+18	+12
Evergreen broadleaf forest	11778	452	499	120	-47	-10	340	130	+111	+25
Deciduous needleleaf forest	2498	104	156	56	-53	-51	29	76	+74	+72
Deciduous broadleaf forest	1106	179	299	145	-120	-67	80	117	+99	+55
Mixed forest	13470	172	220	59	-48	-28	127	66	+45	+26
Shrublands <sup>1</sup>	29542	69	116	63	-47	-68	64	64	+5	+7
Savannas <sup>2</sup>	18846	162	246	107	-84	-52	107	79	+55	+34
Grasslands	21844	76	146	83	-70	-93	97	58	-22	-29
Croplands	12417	116	174	89	-58	-50	97	55	+19	+16
Croplands and natural vegetation mosaic	5782	166	243	108	-77	-46	112	89	+54	+33
Global <sup>3</sup>	-	128	183	-	-	-44	109	-	-	+15

<sup>1</sup>including open and closed shrublands. <sup>2</sup>including woody savannas and savannas. <sup>3</sup>for overlapped pixels with 1.5°×1.5° resolution.

**Table 5-** Comparison of transpiration estimated by Gerrits' model to STEAM and GLEAM through Average, RMSE, MBE and RE per land cover type. Negative MBE and RE show the Gerrits' model underestimates evaporation and vice versa. Average, RMSE and MBE are in mm year<sup>-1</sup> and RE is in %.

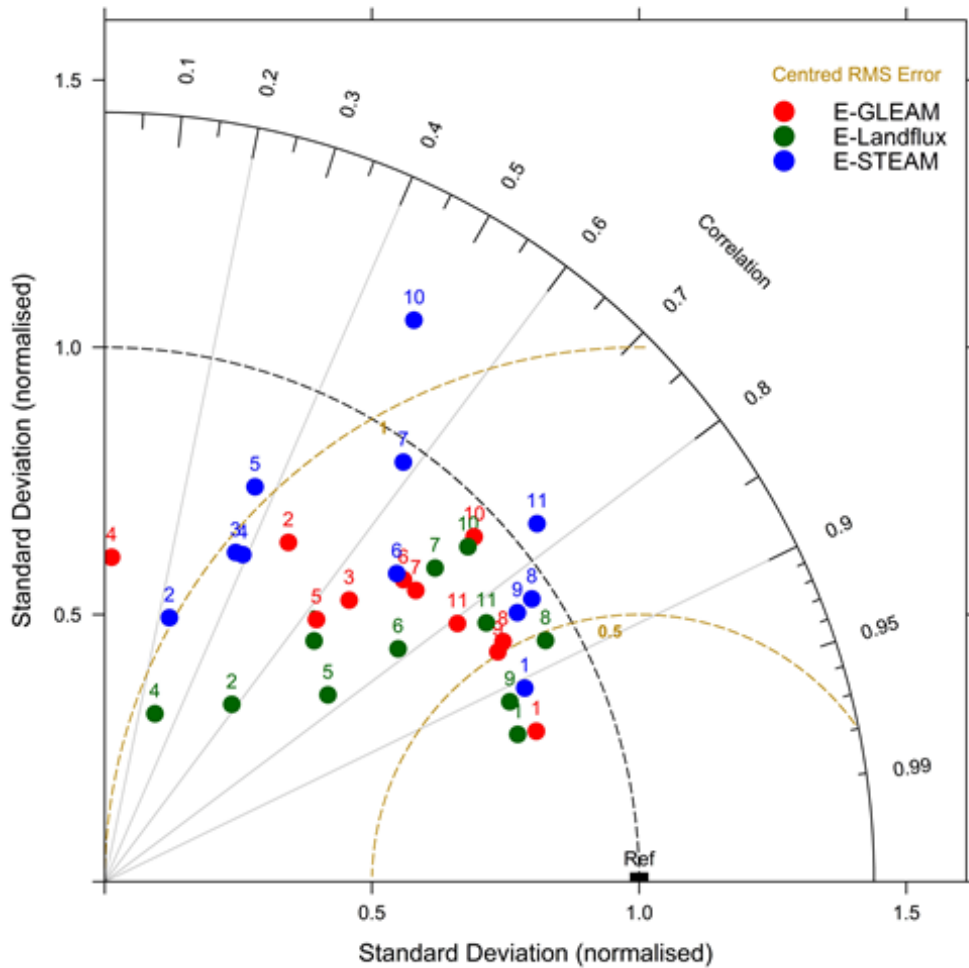
Land cover	Area	Gerrits	STEAM				GLEAM			
	1000 km <sup>2</sup>	Avg.	Avg.	RMSE	MBE	RE	Avg.	RMSE	MBE	RE
Evergreen needleleaf forest	5563	284	222	122	+63	+22	259	100	+25	+9
Evergreen broadleaf forest	11778	915	619	347	+296	+32	890	163	+25	+3
Deciduous needleleaf forest	2498	234	177	82	+57	+24	261	71	-21	-12
Deciduous broadleaf forest	1106	617	538	192	+79	+13	570	120	+47	+16
Mixed forest	13470	390	305	147	+85	+22	363	114	+27	+7
Shrublands <sup>1</sup>	29542	133	137	85	+4	+3	159	81	-26	-20
Savannas <sup>2</sup>	18846	533	473	162	+59	+11	577	148	-44	-8
Grasslands	21844	199	214	109	+15	+7	233	93	-34	-17
Croplands	12417	372	393	131	-20	-5	371	90	+1	0
Croplands and natural vegetation mosaic	5782	521	444	159	+77	+15	530	112	-10	-2
Global <sup>3</sup>	-	315	276	-	-	+12	329	-	-	-4

<sup>1</sup>including open and closed shrublands. <sup>2</sup>including woody savannas and savannas. <sup>3</sup>for overlapped pixels with 1.5°×1.5° resolution.



1

2 **Figure 1-** Mean annual evaporation estimated by (a) Gerrits' model, (b) Landflux-EVAL  
 3 (Mueller et al., 2013), (c) STEAM (Wang-Erlandsson et al., 2014, Wang-Erlandsson et al., 2016)  
 4 and (d) GLEAM (Martens et al., 2017; Miralles et al., 2011a).



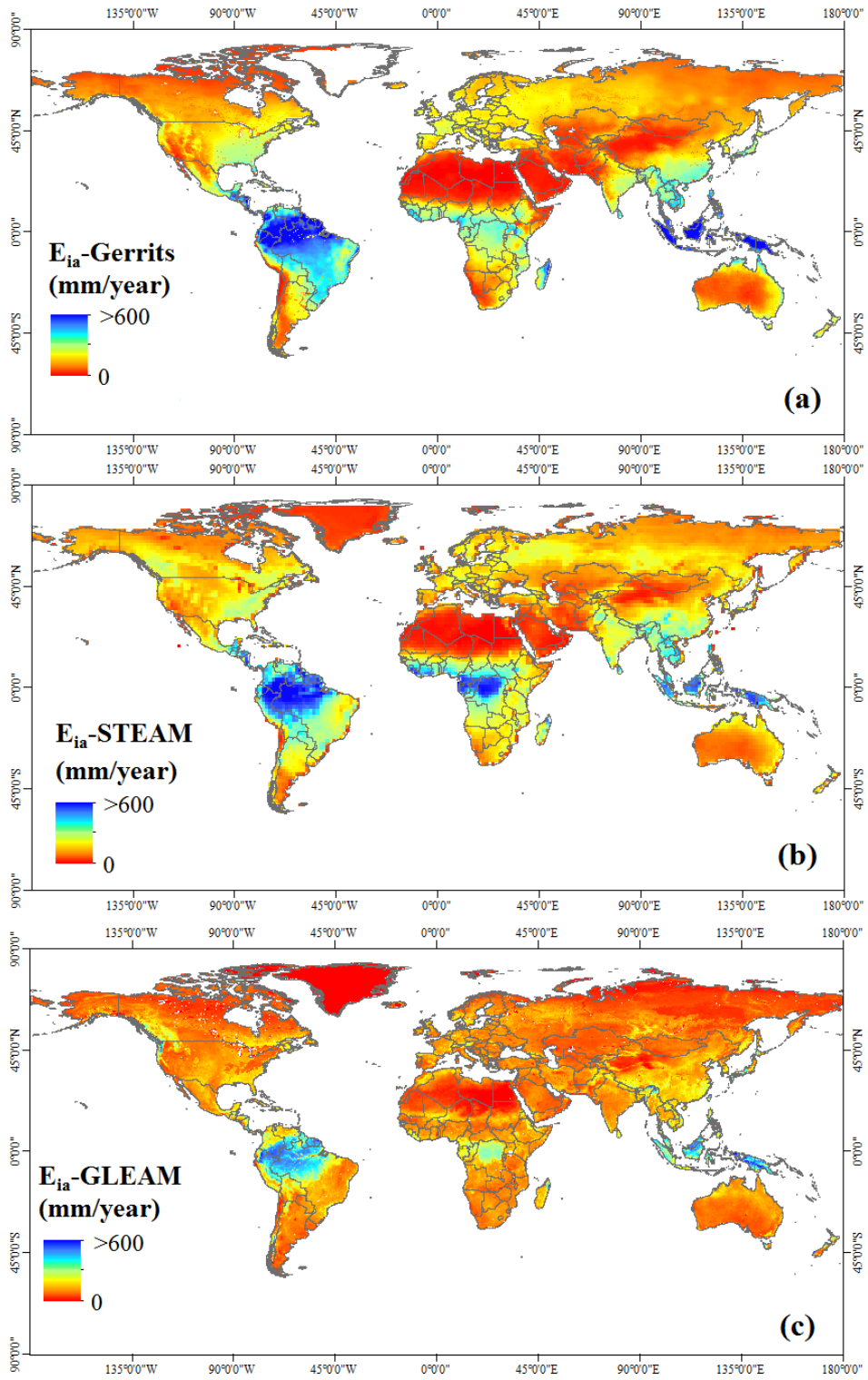
1

2 **Figure 2-** Taylor diagram for mean annual evaporation estimated by Gerrits' model in  
 3 comparison to Landflux-EVAL (green circles), STEAM (blue circles) and GLEAM (red circles)  
 4 for all data (No. 1), Evergreen Needleleaf Forest (No.2), Evergreen broadleaf forest (No. 3),  
 5 Deciduous needleleaf forest (No. 4), Deciduous broadleaf forest (No. 5), Mixed Forest (No. 6),  
 6 Shrublands (No. 7), Savannas (No. 8), Grasslands (No. 9), Croplands (No. 10) and Croplands  
 7 and natural vegetation mosaic (No. 11).

8

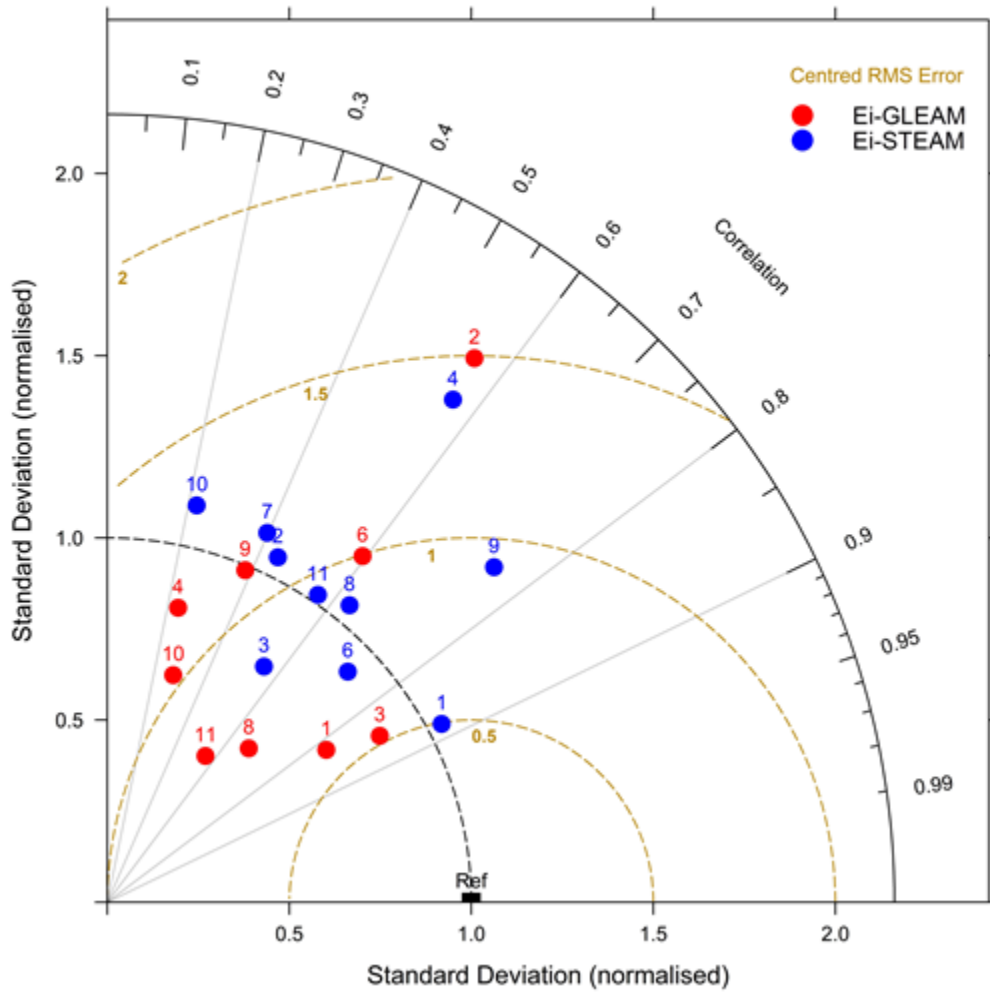


1



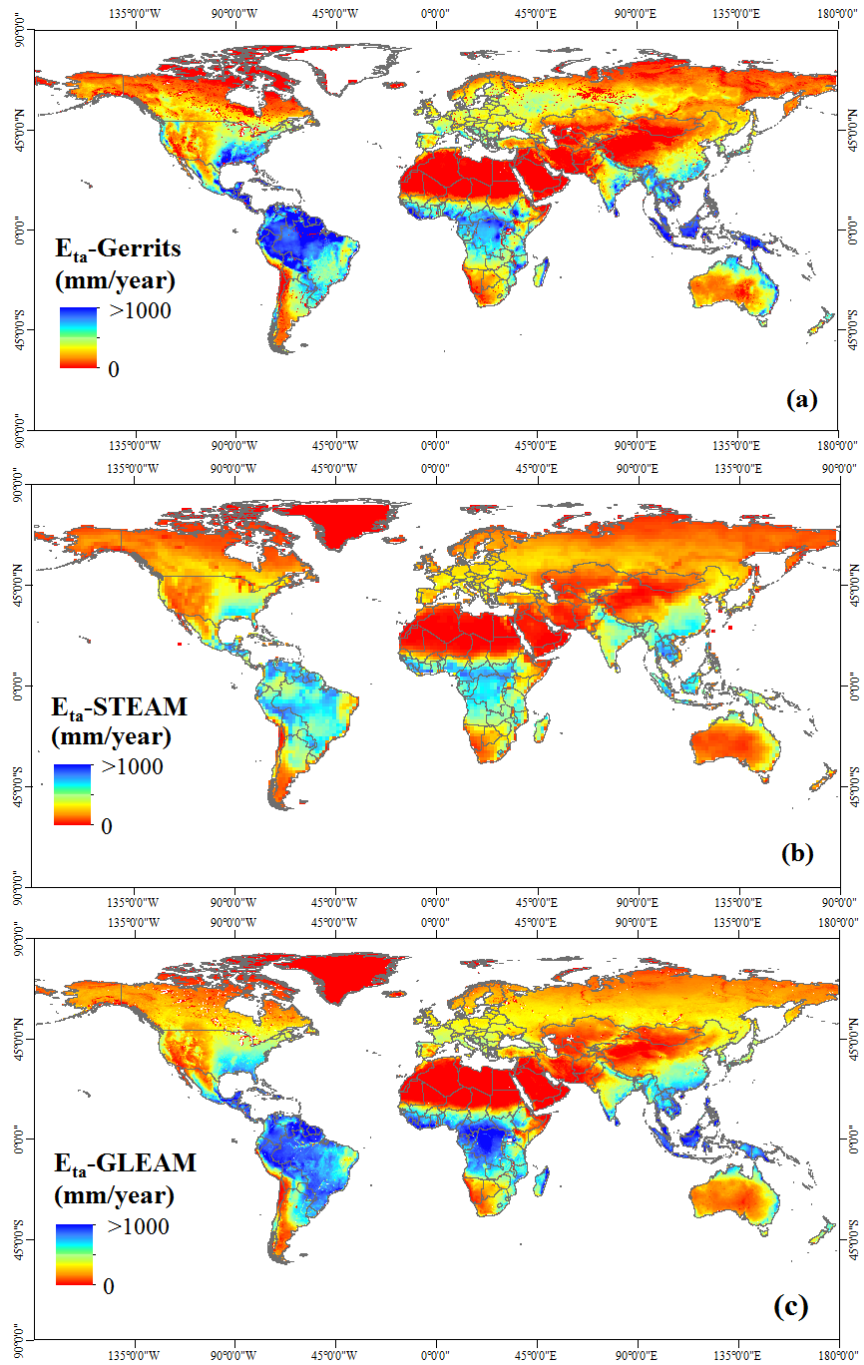
2

3 **Figure 3-** Simulated mean annual interception by (a) Gerrits' model and (b) STEAM and (c)  
4 GLEAM.

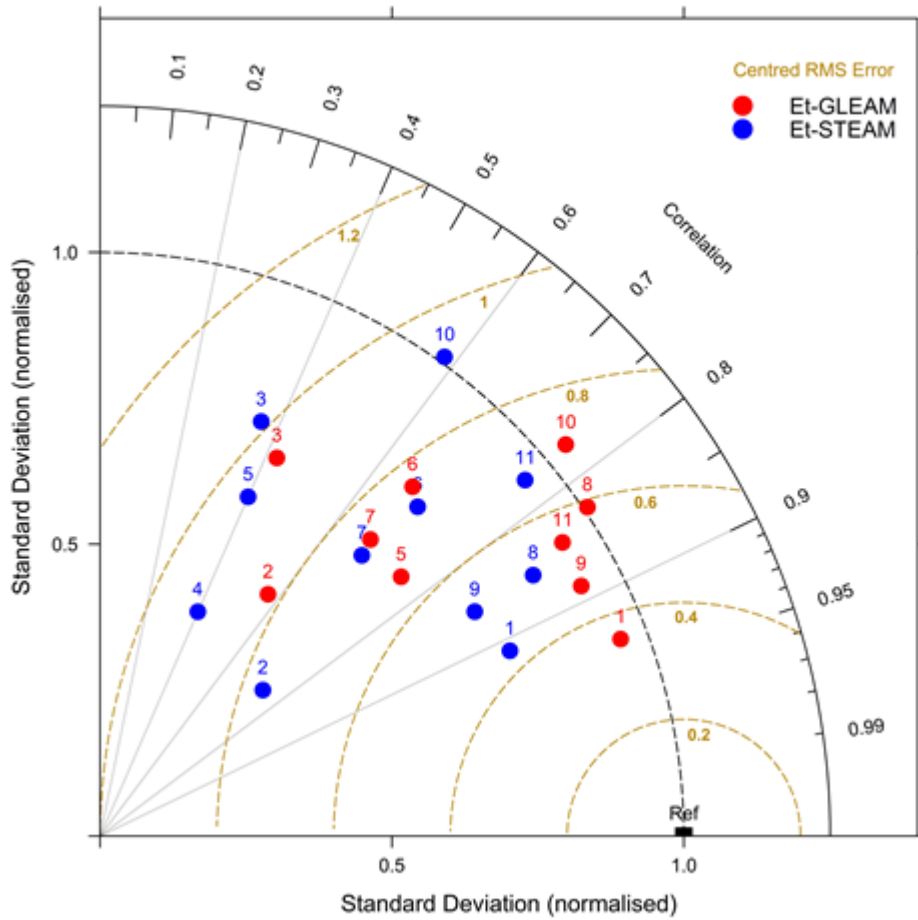


1  
 2 **Figure 4-** Taylor diagram for mean annual interception estimated by Gerrits' model in  
 3 comparison to STEAM (blue circles) and GLEAM (red circles) for all data (No. 1), Evergreen  
 4 Needleleaf Forest (No.2), Evergreen broadleaf forest (No. 3), Deciduous needleleaf forest (No.  
 5 4), Deciduous broadleaf forest (No. 5), Mixed Forest (No. 6), Shrublands (No. 7), Savannas (No.  
 6 8), Grasslands (No. 9), Croplands (No. 10) and Croplands and natural vegetation mosaic (No.  
 7 11).

8



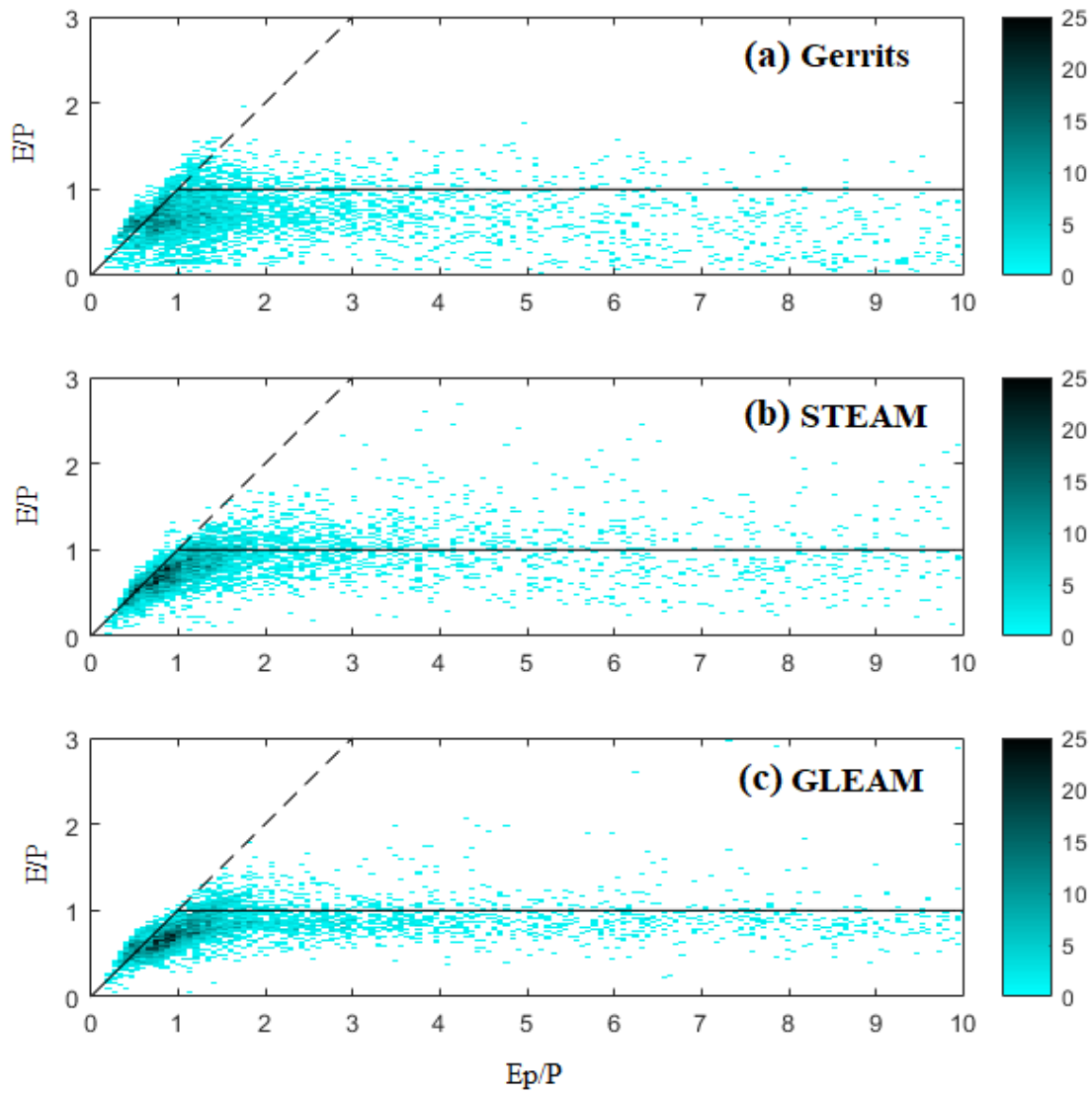
1  
 2 **Figure 5-** Simulated mean annual transpiration by (a) Gerrits' model, (b) STEAM and (c)  
 3 GLEAM.



1

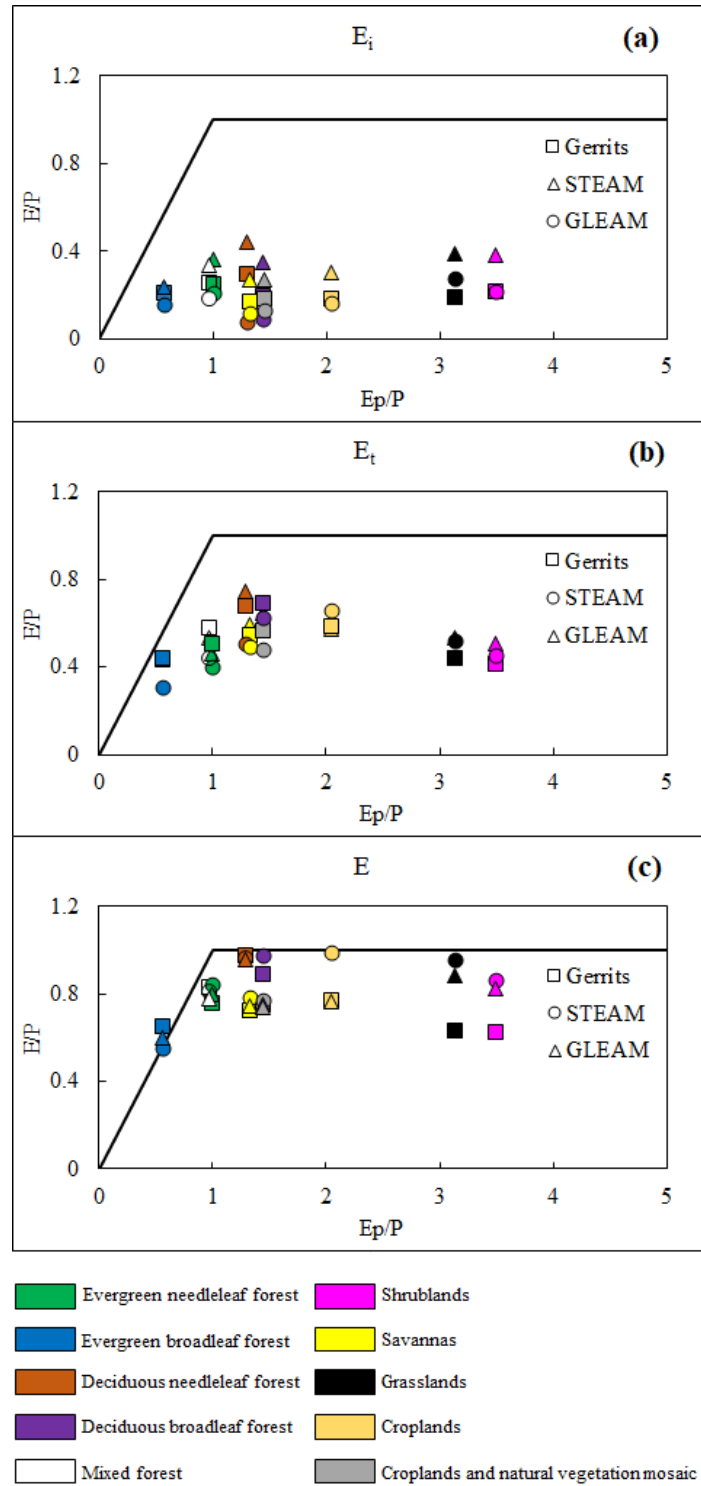
2 **Figure 6-** Taylor diagram for mean annual transpiration estimated by Gerrits' model in  
 3 comparison to STEAM (blue circles) and GLEAM (red circles) for all data (No. 1), Evergreen  
 4 Needleleaf Forest (No.2), Evergreen broadleaf forest (No. 3), Deciduous needleleaf forest (No.  
 5 4), Deciduous broadleaf forest (No. 5), Mixed Forest (No. 6), Shrublands (No. 7), Savannas (No.  
 6 8), Grasslands (No. 9), Croplands (No. 10) and Croplands and natural vegetation mosaic (No.  
 7 11).

8



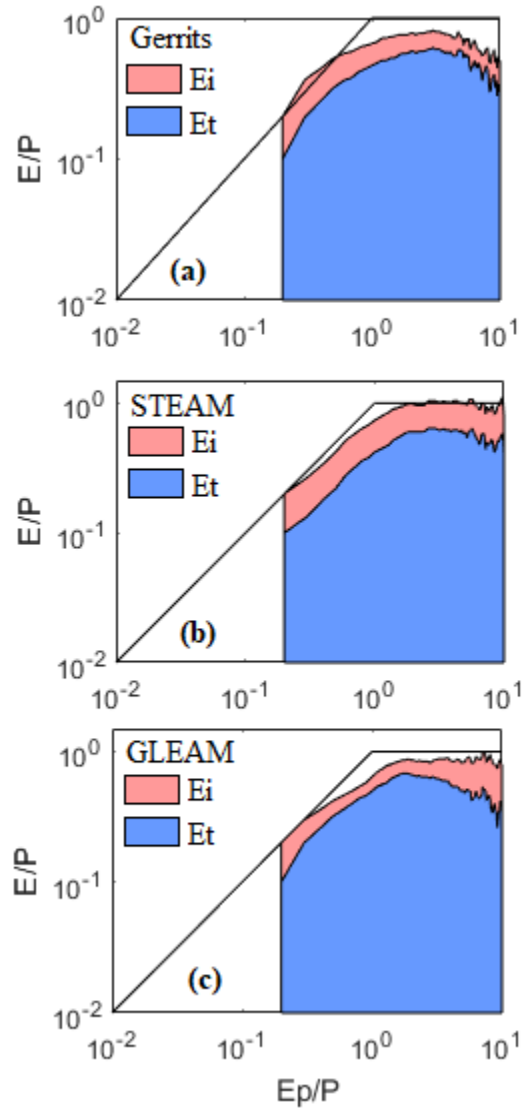
1

2 **Figure 7-** Density plot of  $\frac{E}{P}$  versus  $\frac{E_p}{P}$  for comparison between models within the Budyko  
 3 framework. The legend shows the frequency of pixels.



1

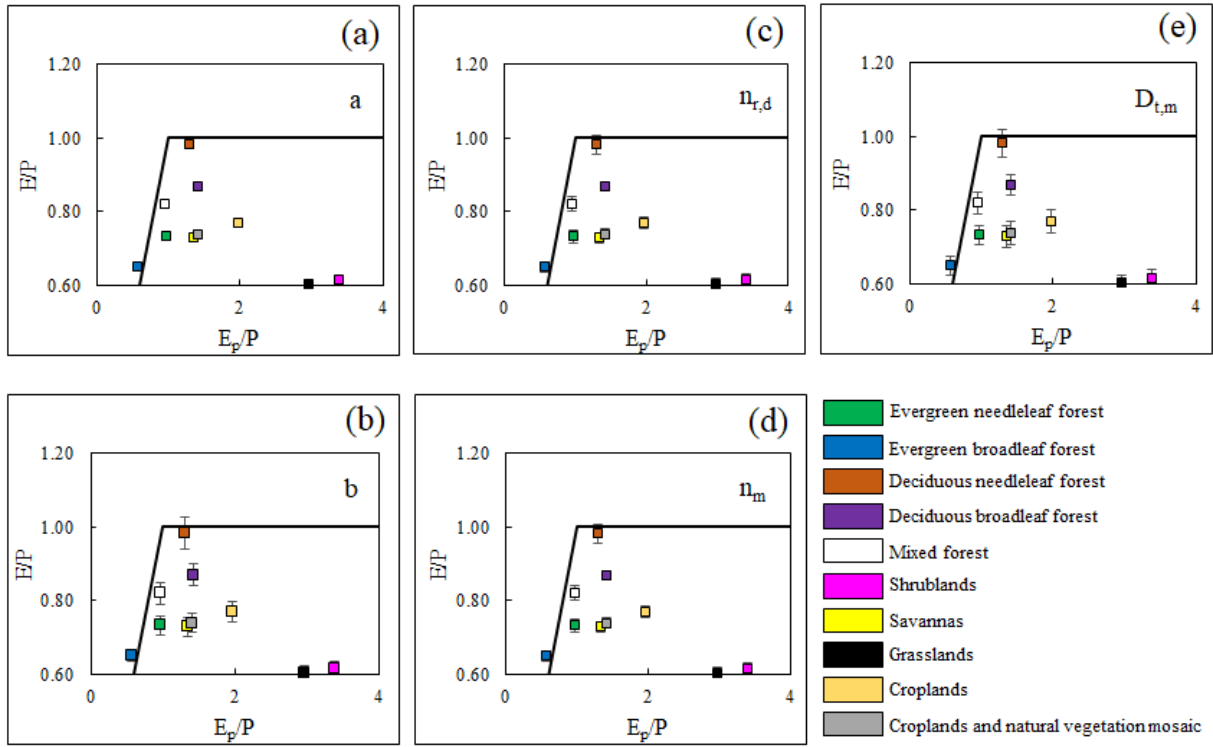
2 **Figure 8-** Comparison of interception (a), transpiration (b) and total evaporation (c) between  
 3 models for each land cover within the Budyko framework.



1

2 **Figure 9-** The distribution of  $\frac{E_i}{P}$  and  $\frac{E_p}{P}$  with respect to aridity for each model.

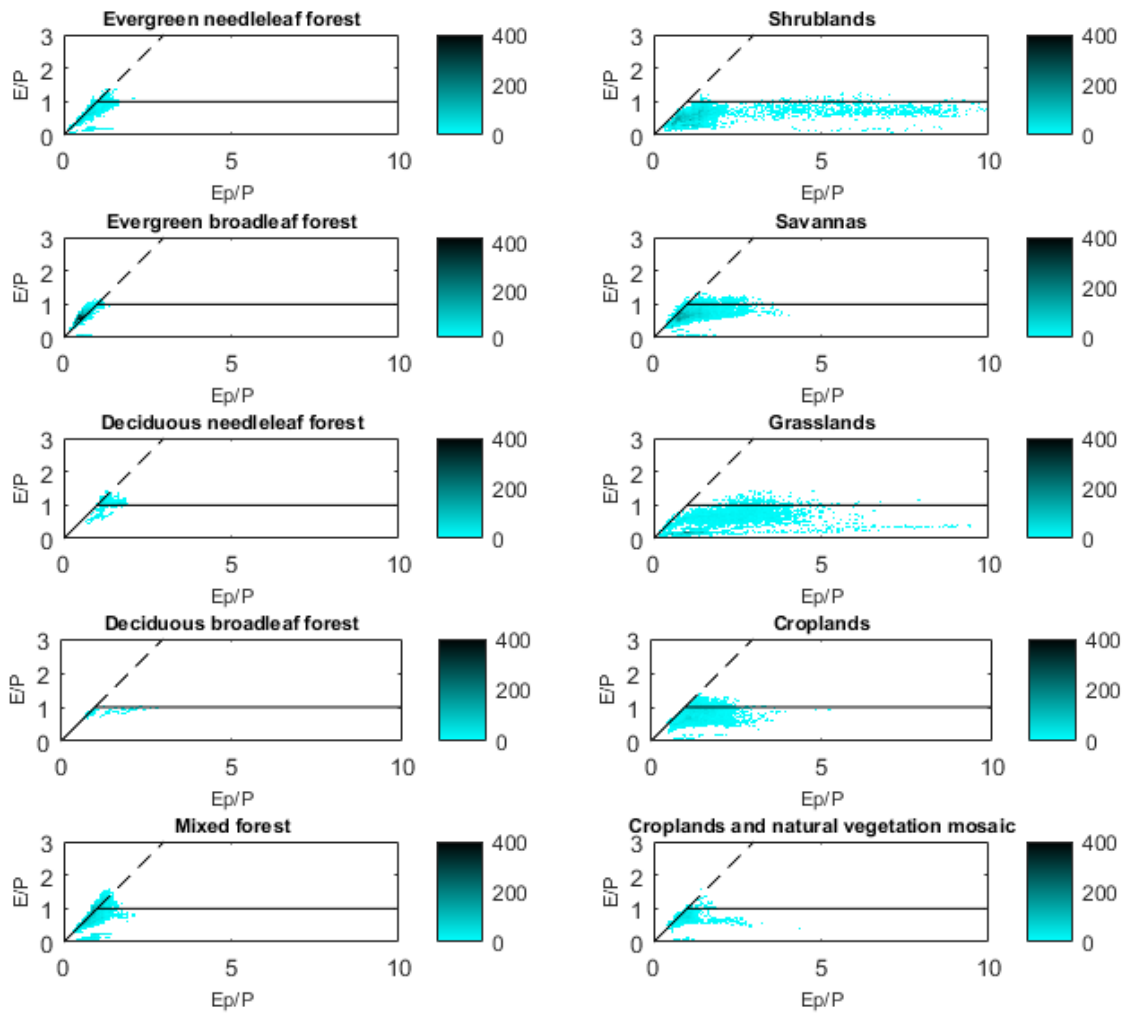
3



1

2 **Figure 10-** Sensitivity analysis of the model to 10% changes in (a) parameter  $a$  in Eq. (18), (b)  
 3 parameter  $b$  in Eq. (8), (c) number of rain days  $n_{r,d}$ , (d) number of rain months  $n_m$ , and (e)  
 4 transpiration threshold  $D_{t,m}$ .





1

2 **Figure 11-** Density plot of  $\frac{E}{P}$  versus  $\frac{E_p}{P}$  for each land cover.